

Mitochondrial Variability as a Source of Extrinsic Cellular Noise

Iain G. Johnston^{1,2}, Bernadett Gaal^{1,3}, Ricardo Pires das Neves^{4,5}, Tariq Enver³, Francisco J. Iborra⁶, Nick S. Jones^{1,2,*}

1 Department of Physics and CABDyN Complexity Centre, Clarendon Laboratory, Parks Road, Oxford, United Kingdom

2 Oxford Centre for Integrative Systems Biology, Department of Biochemistry, South Parks Road, Oxford, United Kingdom

3 UCL Cancer Institute, University College London, Gower Street, London, United Kingdom

4 Center for Neuroscience and Cell Biology, University of Coimbra, 3004-517 Coimbra, Portugal

5 Biomaterials and Stem Cell-based Therapeutics Group and Biocant – Center of Innovation and Biotechnology, 3060-197 Cantanhede, Portugal

6 Department of Molecular and Cellular Biology, Centro Nacional de Biotecnología, Consejo Superior de Investigaciones Científicas, Madrid, Spain

* Email: n.jones1@physics.ox.ac.uk

Abstract

We present a study investigating the role of mitochondrial variability in generating noise in eukaryotic cells. Noise in cellular physiology has been found to play an important role in many fundamental cellular processes, including transcription, translation, stem cell differentiation and response to medication. However, the mechanisms through which random influences affect these processes have yet to be clearly elucidated. Here we present a mechanism by which variability in mitochondrial volume and functionality is linked to variability in transcription rate and hence has a profound effect on downstream cellular processes. We expose a knitting of cell cycle variability, transcription rate variation and mitochondrial variation. Our model mechanism is supported by an appreciable volume of recent experimental evidence, and we present the results of several new experiments with which our model is also consistent. We find that noise due to mitochondrial variability can sometimes dominate over other extrinsic noise sources (such as cell cycle asynchronicity) and can significantly affect large-scale observable properties such as cell cycle length. We also explore two recent regulatory network-based models for stem cell differentiation, and find that extrinsic noise in transcription rate causes significant variability in the behaviour of these model systems. These results suggest that mitochondrial and transcriptional variability may be an important mechanism influencing a large variety of cellular processes and properties.

Author Summary

Mitochondria are the energy-producing components of cells, and the number and functionality of mitochondria in cells varies throughout a population. Cellular variability has been found to play a major role in diverse and important phenomena, including stem cell differentiation and drug resistance, but the sources of this variability have yet to be satisfactorily explained. We propose a mechanism, supported by a substantial number of recent and new experiments, by which mitochondrial variability causes variability in transcription rate between cells and may hence be a significant source of noise in protein levels in many downstream processes. The mitochondrial variability the data leads us to consider is a mix of two factors, not only the amount of mitochondria in the cell, but also a measure of their quality. We illustrate the downstream effect of mitochondrial variability through simulated studies of protein expression and stem cell differentiation, and suggest possible experimental approaches to further elucidate this mechanism.

Introduction

Stochastic influences significantly affect a multitude of processes in cellular biology [1–5]. Understanding the sources of this randomness within and between cells is a central current challenge in quantitative biology. Noise has been found to affect processes including stem cell fate decisions [6], bet-hedging in bacterial phenotypes [7,8], cancer development [9], and responses to apoptosis-inducing factors [10,11]. In this paper, we consider how mitochondria may constitute a significant source of this cellular noise.

Noise in cellular processes may result from sources intrinsic to the gene in question (those responsible for differences in the expression levels of genes under identical regulation in the same cell) or extrinsic sources (those responsible for cell-to-cell variation in genes under identical regulation in a population). Both intrinsic and extrinsic noise sources contribute to the overall noise observed in, for example, transcription rates and protein expression levels [12]. The interplay between intrinsic and extrinsic noise can be characterised with elegant experimental techniques such as dual reporter measurements [3], in which the expression levels of two proteins are measured within cells and within a population. Some studies have found the contribution of extrinsic factors to overall noise levels to be stronger in eukaryotes [13,14] than prokaryotes [3], although others debate this interpretation [15]. To investigate these influences, several mathematical models for the emergence of intrinsic and extrinsic cellular noise have been introduced and explored [12,16–23]. In addition, recent studies have investigated, both experimentally and theoretically, the architecture of extrinsic noise and its causal factors [13–15,18,24–26], though substantial uncertainty surrounds the importance of individual contributions (such as cell cycle stage and cellular volume) to extrinsic noise [27].

Huh and Paulsson recently argued that uneven segregation of cellular constituents at mitosis can contribute significantly to cell-to-cell differences in levels of cellular components and proteins in a population, focusing on stochasticity in protein inheritance between sister cells [28]. An experimental study performed by das Neves *et al.* identified uneven partitioning of mitochondria at mitosis as being a possibly significant source of extrinsic noise in eukaryotes [29]. Mitochondria have been found to display remarkably complex behaviour interwoven with cellular processes [30–32] and to display significant heterogeneity within cells [29, 33–35]. Mitochondrial influences on processes including stem cell differentiation [36] and cell cycle progression [37–39] have recently been observed.

das Neves *et al.* [29] observe a wide spread of mitochondrial masses in a population of cells, illustrating extrinsic variability in organelle distribution. Mitochondrial functionality has also been observed to vary between cells [32, 33, 40–42]. das Neves *et al.* also observed a link between mitochondrial mass and membrane potential and cellular ATP levels, and found transcription rate to be a function of ATP concentration. In addition, the modulation of mitochondrial functionality, through anti- and pro-oxidant treatments, was found to alter cell-to-cell variability in transcription rates, with anti-oxidants significantly reducing variability and pro-oxidants increasing variability. These results suggest that cell-to-cell heterogeneity in mitochondrial mass and functionality may propagate into extrinsic noise in transcription rate, and thenceforth processes further downstream, but the quantitative links behind these processes remain unclear. We introduce a simple approach, consistent with a range of experimental observations, that quantitatively connects all these features and predicts the downstream physiological influence of mitochondrial variability.

Shahrezaei *et al.* [43] have recently shown that extrinsic noise can influence levels of intrinsic noise, as cell-to-cell variability in the rates of processes such as transcription and translation affect the intrinsic dynamics of gene expression. In addition, they provided an important extension to standard stochastic simulation techniques to allow this variability in the production rates of chemical species to be accurately simulated. However, this theoretical study did not attempt to characterise the physiological causes of this extrinsic noise – an important consideration in assessing the ubiquity and consequences of cellular noise. Our proposal that cell-to-cell mitochondrial variability provides a significant source of extrinsic noise in transcription addresses these causes, and we show that extrinsic noise resulting from mitochondrial variability could significantly influence intrinsic noise in gene expression.

This paper will proceed as follows. We first introduce one of the simplest possible mathematical models for mitochondrial mass and functionality during the cell cycle, and show that it is consistent with a wide range of experimental data, both from the literature and newly reported here, and allows analytical treatment. Our model includes stochastic segregation of mitochondria at mitosis and functional differences in mitochondria between cells, and contains a simple dynamic description of the time evolution of cellular volume and mitochondrial mass through the cell cycle. To our knowledge it is the first model of its kind which links mitochondrial mass and function to the cell cycle and gene expression. We relate mitochondrial properties to the production of ATP in the cell, which in turn affects transcription rates: hence, variability in mitochondrial properties causes downstream variability in transcription. Next, we incorporate the behaviour produced by our model into a common framework for cellular noise, and show that extrinsic noise due to variation in $[ATP]$ can have a profound effect on gene expression levels, dominating over intrinsic noise. We then demonstrate the cell physiological implications of energy variability by showing how mitochondrial variability may affect stem cell differentiation. Finally, we discuss how our model relates to recent work characterising sources of extrinsic noise, and suggest experiments to allow more refined models.

Model

While the heterogeneity of mitochondria has been observed experimentally and connected to variability in processes like transcription [29] and stem cell differentiation [36], the mechanisms by which mitochondrial variability influences other cellular processes has not been elucidated clearly. Here, we describe a simple model which formalises these links, and note that it reproduces recent experimental results concerning mitochondrial heterogeneity and variability in connected cellular features [29]. The simplicity of our model means that analytic expressions can be derived for many quantities of interest, facilitating a more complete and intuitive understanding of the modelled biological connections. We will then use this model to investigate more specific questions regarding the links between mitochondrial variability and transcription rate and stem cell differentiation.

Cellular Dynamics

An individual cell in our model has three key variables: the volume of the cell (v); the amount of mitochondrial mass in the cell (n); and the degree of mitochondrial functionality (f). This last quantity, f , represents a coarse-grained measure of the efficiency of mitochondria within a cell – a factor which may be affected, for example, by the levels of reactive oxygen species (ROS), mitochondrial membrane potential, variability in mitochondrial protein complex abundance, and genetic differences between mitochondria [44].

Our models for cell cycle dynamics consists of equations governing the time evolution of these quantities coupled with a description of the process of mitosis. In the light of a recent study [45], and as cell cycle models often assume the exponential growth picture, we expect an exponential form for cell volume growth: $\dot{v} = \alpha v F(v, n, f)$. Here, $F(v, n, f)$ is a function expressing the dependence of volume growth rate on other parameters.

We suggest that ATP concentration ($[ATP]$) plays a key role in powering growth of the cell. Ref. [29] found ATP levels in the cell to be proportional to mitochondrial mass (n) and membrane potential (a factor that may be absorbed into our measure of

‘mitochondrial function’ f), so we write $[ATP] = \gamma n f / v$, so that $F(v, n, f) = [ATP]$. The meaning of f now becomes apparent as a scalar multiple relating mitochondrial density to $[ATP]$. We note that other choices for the form of $[ATP]$, including ODEs, are possible, and explore some alternatives in ‘ATP & Transcription Noise’ (Supplementary Information).

We note that although ATP concentration has been suggested [29] as a possible mechanism linking mitochondria and transcription rate, and some evidence supports this link, it may be the case that a different factor provides the causal mechanism, and ATP concentration is correlated with this underlying factor. For example, ROS, which adversely affect many cellular processes, may be an alternative to ATP, or a combination of ATP and ROS levels may act to determine transcription rate.

Numerous historical studies, both in HeLa cells [46] and other tissue types [47–52] have found that the density ρ of mitochondrial mass (also called mitochondrial volume density) within cells of a given tissue type is consistent between generations and within populations. This consistency suggests that the time evolution of mitochondrial mass should be (a) coupled with the time evolution of volume and (b) of a form that allows damping of the inherent stochasticity at mitosis. In addition to these features, it is presumably reasonable to assume that mitochondrial growth is dependent on available $[ATP]$ (due to the required protein synthesis). We suggest a model that captures these required dependencies and incorporates mean-reversion, given by the dynamic equations: $\dot{v} = \alpha f \rho v$, $\dot{n} = \beta f \rho v$, where $\rho = n/v$.

Our mitochondrial mass measure n physically represents total mitochondrial volume. However, it will be of use when considering the segregation of mitochondria at mitosis to consider the cell as populated by a number of discrete ‘virtual’ mitochondria. We denote these entities as ‘virtual’ mitochondria due to the difficulty of regarding mitochondria as individuals given the processes of fission and fusion. The system as chosen is scaled so as to regard n as mitochondrial copy number, so that, if n is measured in μm^3 , each ‘virtual’ mitochondrion possesses a default volume of $1 \mu m^3$ (see Methods). These virtual mitochondria are the discrete elements that are binomially partitioned at mitosis, as outlined in the next subsection.

The model’s dynamics result (see Methods) in a convergence in mitochondrial density with time to a value β/α .

Mitochondrial Function & Behaviour at Mitosis

Cells undergo mitosis when their volume reaches a cutoff v^* . When this occurs, the cell divides in two, with mitochondrial mass n split stochastically between daughter cells, with each unit of mass being assigned to each cell with equal probability, and cell volume also segregated similarly (see Methods). In our model, the partitioning of n and v at mitosis is uncorrelated. While this may not be the case in biology (larger daughter cells may be expected to inherit more mitochondria) we lack experimental evidence to quantify this correlation and so choose the uncorrelated situation for simplicity. This model was chosen as the most straightforward representation of stochastic division of discrete elements (the ‘virtual mitochondria’ mentioned in the last section) and is likely to represent a realistic scenario if there is no explicit biological control mechanism that modulates the distribution of inherited mitochondria.

We note that a feature of our model initially contrasts with another experimental observation: specifically, that differences in cells that arise at mitosis are damped out by the subsequent dynamics. By contrast, Ref. [29] finds that noise levels in mRNA synthesis are observed to be higher in a bulk population than between sister cells, suggesting that significant variability still exists despite these damping dynamics, which on their own would lead us to expect sister cells, post-mitosis, to exhibit the greatest possible variation. Another observation indicates a solution to this problem: populations of cells treated with antioxidants, which improve mitochondrial functionality, showed a significant drop in noise levels. This result suggests that an extra source of noise, functional variability between cells, may be responsible for increasing noise levels.

We consider the variable f to be the degree of functionality of a cell’s mitochondria. das Neves *et al.* show that a measure of mitochondrial functionality (membrane potential) is slowly-varying with time in a given cell, although there is a wide distribution of functionality within a population [29]. It was also found that sister cells have similar transcriptional noise levels. In the absence of a more refined view of functionality, we assume that all changes in functionality occur at division and that f stays constant through the cell cycle. f changes in a stochastic but mean-reverting fashion at division, and both daughters receive the same f value (see Methods for more detail).

$[ATP]$ and Transcription Rate

We are interested in the time evolution of $[ATP]$. Ref. [29] has $[ATP]$ scaling with the total mass of mitochondria in a cell [29]. This observation motivates our choice of expression for ATP concentration, $[ATP] = \frac{\gamma n f}{v}$. das Neves *et al.* also show a link between the total transcription rate λ in a cell (measured through bromouridine incorporation across the whole nucleus) and $[ATP]$, a sigmoidal curve, which we approximate (see ‘Parameterisation of $\lambda(t)$ ’ in Supplementary Information) with $\lambda = s_1 + s_2 \tan^{-1}(s_3[ATP] + s_4)$.

das Neves *et al.* record a change in the structure of this sigmoid curve in experiments where cellular chromatin is artificially decondensed. In these situations, the sigmoidal response of λ to $[ATP]$ becomes a hyperbolic curve, with a sharp, continuous increase of λ with $[ATP]$ at low $[ATP]$. This change may reflect the necessity of remodelling chromatin – a process that requires ATP – for the transcription process. Chromatin remodelling has been noted by several studies [14, 15, 21] to play an important role in mRNA synthesis noise and hence downstream noise in gene expression. Rather than attempting to model this influence explicitly, we use the experimentally-determined form for $\lambda([ATP])$ to capture the overall dependence of transcription rate (including chromatin effects) on $[ATP]$.

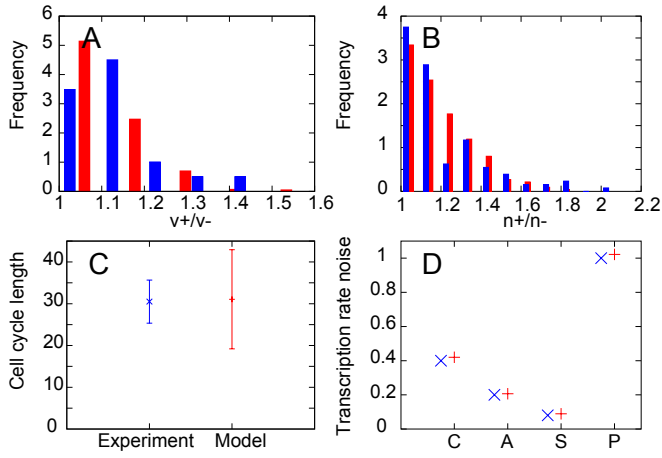


Figure 1: **The set of data used to parameterise our model.** Experimental data shown in blue, fitted simulated data shown in red. A. Ratio of larger cell volume to smaller cell volume between sisters at birth. B. Ratio of larger mitochondrial mass to smaller mitochondrial mass between sisters at birth. C. Mean and standard deviation of the cell cycle length in a population of cells. D. Noise levels in transcription rate in (C)ontrol, (A)ntioxidant-treated and (P)ro-oxidant-treated populations, and between (S)ister cells. Two other experimental values, not pictured, that were used to parameterise our model are a maximum cell volume of $2500 \mu\text{m}^3$ (for consistency with Ref. [45]) and a mean ATP concentration of $900 \mu\text{M}$ (from Ref. [53]).

Results

Our simple model is sufficient to reproduce a large set of experimental data

Values for the parameters in our model were chosen (see Methods) to match a subset of experimental data, illustrated in Fig. 1. We then confirmed the biological applicability of our simple model by comparing the behaviour it predicts to recent experimental data from das Neves *et al.* [29]. Henceforth, we will refer to figures in the das Neves *et al.* study [29] as e.g. N1a for Fig. 1a.

Distributions of mitochondrial mass and cell volume. Our model gives a peaked distribution skewed towards low n values for mitochondrial mass in the bulk population (Fig. 2A), which is similar in form to the experimental distribution (N4b). The distribution of cellular volumes in a bulk population (Fig. 2B) is found to display the quadratic decay expected from a theoretical treatment of cells growing exponentially [18].

Weak correlation between the lengths of successive cell cycles in a population. Fig. 2C shows the weak relationship between the cell cycle length of a parent and a daughter cell, which qualitatively matches experimental findings (from N4h).

Mitochondrial mass at birth is a better predictor of cell cycle length than cell volume at birth. Figs. 2D and 2E illustrate the correlations between cell cycle length and a cell's birth values of n and v respectively. The correlation between birth mitochondrial mass and cell cycle length was strong ($R^2 = 0.69$, compared to the experimental value of 0.78) compared to the correlation between birth cell volume and cell cycle length ($R^2 = 0.28$, experimental value 0.22). The same correlation behaviour is observed in experiments (from N4e and N4f) which are shown for comparison.

Transcription rate noise with cell cycle stage. We modelled progression through the cell cycle stages by assigning stages according to the volume v of a cell. We assign cells with $0.5v^* \leq v < 0.7v^*$ to G_1 , $0.7v^* \leq v < 0.95v^*$ to S , and $0.95v^* \leq v < v^*$ to G_2 stages, to approximate the proportion of total cell cycle length that HeLa cells are observed to spend in each stage [54]. Transcription rate noise was found to stay relatively constant (around 0.4) when population subsets at different positions in the cell cycle were measured (see Fig. 2F), as observed in experiments (NS1).

Correlation between mitochondrial mass and cell volume. Our model predicts a strong correlation between cell volume v and mitochondrial mass n (Fig. 2G). This result contrasts with the weak correlation observed, using forward scatter in flow cytometry to measure volume, by das Neves *et al.* (N3a) (we confirmed these experimental results in this study – data not shown). However, many historic studies have found a much stronger connection between mitochondrial mass and cellular volume. The mitochondrial density $\rho = n/v$, also referred to as mitochondrial volume density, has been found to exhibit low standard deviation (between 0.01 and 0.15 of the mean) in many different mammalian tissue types [46–52] and amounts of mtDNA have been found to display similarly low variability [47, 55]. These results contrast with the extremely high variability in mitochondrial volume density observed by das Neves *et al.* (the noise level estimated from the data is around 0.32). We choose our model, noting that flow cytometry data (while useful for providing approximate orderings of cells by volume) may not be capable of providing the absolute volume measurements which are required to recapitulate the low variability in ρ observed elsewhere.

Distribution of transcription rate per unit volume. Fig. 2H shows the distribution of transcription rate per unit nuclear volume (in our model, nuclear volume is taken as proportion to cell volume) in the bulk population. This result follows a similar peaked distribution to that found experimentally (N1a).

We also note some qualitative features of our model: an increase in transcription rate with ATP levels is observed (trivially due to the functional form of λ), which is also observed experimentally (N3g). We also observe an increase in transcription rate per unit volume with total mitochondrial functionality (nf in our model), found experimentally (N3d). Fig. 3 shows illustrative

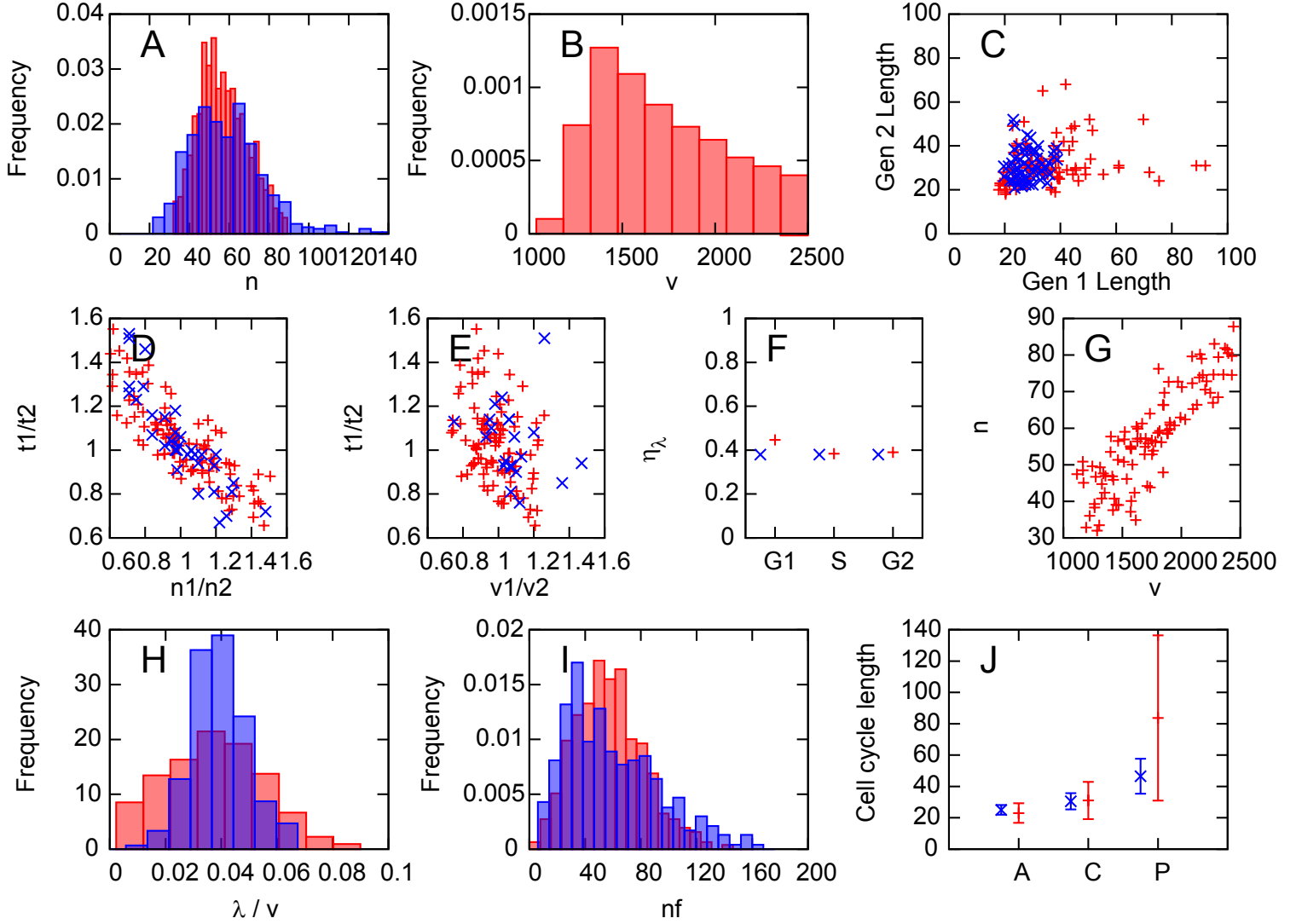


Figure 2: **Our simple model is consistent with experimental probes of mitochondrial and cellular variability.** Comparison between our model (red) and experimental data (blue), following discussion in the Main Text. **Experimental data from das Neves *et al.* [29].** A. Distribution of mitochondrial mass n in an unsynchronised population of cells. B. Distribution of cell volume v in an unsynchronised population of cells. C. Comparison of the lengths of cell cycles between generations: Gen 1 is the parent cell, Gen 2 the daughter. Cell cycle lengths are only weakly correlated. D. Relationship between the ratio of mitochondrial masses at birth against ratio of cell cycle lengths for sister pairs. E. Relationship between the ratio of cellular volumes at birth and the ratio of cell cycle lengths for sister pairs, showing a weaker correlation than D. F. Transcription rate noise η_λ in subsets of the population in G_1 , S , and G_2 phases (see Main Text). G. Mitochondrial mass n and cell volume v are strongly correlated in our model. Some experimental evidence is contradictory (see Main Text). H. Distribution of transcription rate per unit volume λ/v . **New experimental data (see Methods).** I. Distribution of total mitochondrial functionality (nf in our model, CMXRos readings from experiments). J. Mean and standard deviation of cell cycle lengths in (A)nti-oxidant-treated, (C)ontrol, and (P)ro-oxidant-treated populations. Experimental histograms, originally presented in arbitrary units, have been scaled to match the mean value of the simulated data.

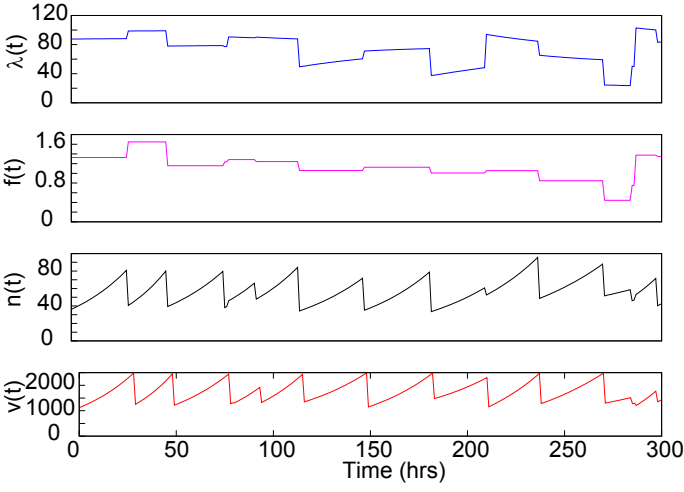


Figure 3: **Illustration of the dynamics of our model.** Example time series of λ (transcription rate), f (mitochondrial functionality), n (mitochondrial mass) and v (cell volume), as a cell grows and divides repeatedly in our model.

time series of the dynamic variables involved in simulation of our model.

New experimental results are also consistent with this model

In Fig. 2, we also present new experimental results pertaining to our model.

Distribution of mitochondrial functionality. Fig. 2I shows the distribution of total mitochondrial functionality in a population of cells. In our model, this distribution is just the distribution of the quantity nf , and in experiments, a close equivalent is total CMXRos signal from single cells, measuring the total membrane potential within a cell (see Methods).

Cell cycle lengths in different oxidative conditions. In Fig. 2J we show the mean and standard deviation of cell cycle lengths in a control population, and upon treatment with anti- and pro-oxidants (see Methods). In our simulations, these treatments are modelled by changing the value of f_c , affecting the mean functionality of mitochondria (see Table 1). It is observed that treatment with anti-oxidants reduces cell cycle lengths, and treatment with pro-oxidants increases cell cycle lengths. In our model, this behaviour emerges from the dependence of the rate of volume growth on $[ATP]$, and the increased $[ATP]$ levels resulting from mitochondria with higher functionality.

Mitochondrial mass and membrane potential. We also observed a linear correlation between total mitochondrial mass (measured with MitoGreen) and total mitochondrial membrane potential (measured with CMXRos) in experiments performed with both dyes (see Methods and ‘Mitochondrial Membrane Potential’ in Supplementary Information). This linear correlation emerges from our model due to our representation of total mitochondrial functionality as the product of a functional measure f with mitochondrial mass n . The observed correlation provides qualitative support for this representation.

The good correspondence between experimental data and the simulated behaviour of our model suggests that, although we have chosen simple functional forms in our model, the resulting behaviour is biologically relevant. However, we note here that our model was constructed from a phenomenological philosophy, with the intention of using experimental results to construct a plausible coarse-grained explanation for the influence of mitochondrial variability on extrinsic noise in general and transcription rate in particular. Our goal was to introduce a simplified but consistent mathematical summary of the data and to use this to motivate further experiments. To this end, we suggest a set of experiments in ‘Potential Experiments for Refinement’ (Supplementary Information) that would support or contribute to further development of this model. We also note that many potential refinements could be made to our model and suggest several other functional forms in ‘Other Models’ (Supplementary Information).

Noise in transcription rate depends on noise in mitochondrial segregation and functionality

We are now in a position to explore the dependence of the level of noise in transcription rate on the stochasticity in mitochondrial mass and function, and subsequent stochasticity in $[ATP]$. We can calculate an expression for the noise in transcription rate, $\eta_\lambda = \frac{\sigma_\lambda}{\mu_\lambda}$, in terms of the standard deviations of other cellular quantities in a population (see Methods). We find that the dominant sources of transcription rate variability in our model are mitochondrial partitioning and functional variability, as opposed to noise due to variability in volume partitioning or cell cycle stage.

The variance in mitochondrial functionality σ_f^2 is a parameter in our model which we may freely vary to match experimental data. Varying σ_n^2 , the variance of the distribution by which mitochondrial mass is partitioned, corresponds to changing the mitochondrial makeup of the cell: lower σ_n^2 corresponds to more mitochondrial elements, each with smaller volume, while higher σ_n^2 corresponds to fewer, larger mitochondrial elements, which are partitioned binomially at mitosis (see Methods). In Fig. 4, the functional dependence of η_λ on mitochondrial variability (σ_n^2 and σ_f^2) is shown, from analytic calculation and from simulation, in Fig. 4. These results show that transcription rate noise is made up of significant contributions from both mitochondrial

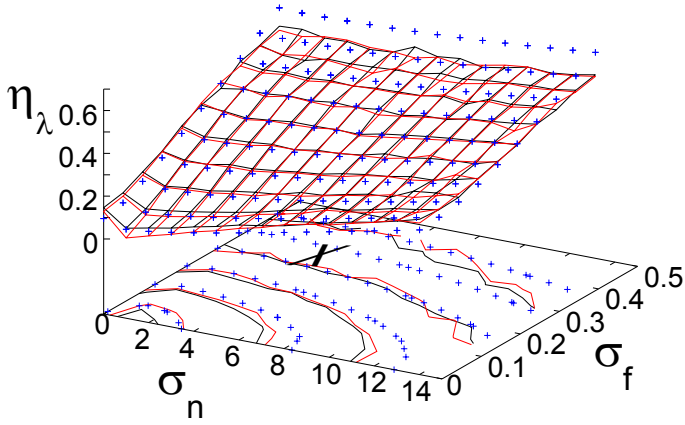


Figure 4: **Variability in mitochondrial mass and functionality can both contribute to noise in transcription rate.** Effects of σ_n , σ_f on transcription rate noise η_λ , from analytic results (blue crosses), simulation with cell volume variability (black lines), and simulation without cell volume variability (red lines). This contour plot shows the value of η_λ for a given combination of σ_n , σ_f according to Eqn. 11 (see ‘Probability Distributions’ in Supplementary Information). Contour lines represent values of $\eta_\lambda = 0.1, 0.2, 0.3, 0.4, 0.5, 0.6$. The ‘X’ mark denotes the default parameterisation of our model. This plot remains essentially identical when variability due to cell age is removed, suggesting that σ_n and σ_f are the controlling variables.

segregation and functionality. This characterisation is a step towards classifying the contributions of different influences to overall extrinsic noise.

The contribution of extrinsic noise due to cell cycle effects in an unsynchronised population can be quantified within this model (see Methods and ‘ATP & Transcription Noise’ in Supplementary Information). A comparison of the two results shows that at the default model values of σ_n and σ_f , the noise in transcription rate is approximately 0.4 amongst a population of unsynchronised cells, and indistinguishable in a population synchronised at a particular age (15 hours). In addition, the variation observed when σ_v , the variability associated with volume partitioning at mitosis, was set to zero is of a much smaller magnitude than the contributions from mitochondrial variability, with the exception of η_λ values at very low values of σ_f and σ_n . These results suggest that, in our model, the majority of extrinsic noise in transcription rate results from variation in mitochondrial segregation and functionality.

Mitochondrial variability can dominate noise in mRNA and protein expression

Having constructed a model for mitochondrial variability and its effect on transcription in the cell, we now investigate the connection between these factors and downstream quantities: mRNA expression levels, and then (through further extension) protein expression levels. Noise in protein expression levels directly affect many cellular properties, as this noise causes cell-to-cell differences in the functional machinery available to perform cellular processes.

The production of mRNA and protein within a cell is often modelled using a master equation approach, addressing the probability of observing a given number of molecules at a given time. This analytical framework lends itself to the inclusion of our results for time-varying transcription rate (see Methods).

We can use Shahrezaei *et al.*’s modification [43] to the Gillespie simulation method [56], allowing for time-varying reaction rates, to simulate this system. This protocol allows us to investigate the relative importance of intrinsic contributions (resulting in differences in expression levels between identical genes within a single cell) and extrinsic contributions (resulting in differences in expression between identical genes in different cells in a population). Fig. 5 shows results from simulations run using (see ‘mRNA & Protein Levels’ in Supplementary Information) a parameter set from Raj *et al.* [15], in two scenarios: one involving only intrinsic noise ($\sigma_n = \sigma_v = \sigma_f = 0$) and one involving extrinsic noise due to mitochondrial mass, functionality, and cell volume variability. In both cases, the initial copy number of mRNA molecules was set to zero, to illustrate differences in the dynamics of the system: transcription started at the birth of the cell, and there were no effects from mRNA inheritance. In the intrinsic noise experiments, a population of cells were simulated from identical initial conditions, with their n, v, f values set to the means of those variables obtained from simulations. The variability in mRNA expression levels in these cells was therefore solely due to intrinsic noise. For the extrinsic noise simulations, mRNA expression was simulated in the heterogeneous population of cells that resulted from dynamic simulation. An ensemble of 2500 cells was analysed for both cases and the mRNA content at each timestep recorded. These simulations allow us to assess the relative importances of intrinsic noise effects (those due to random birth and death processes) and extrinsic effects (those due to the between-cell differences in mitochondrial properties and cell volume). It can be seen that mitochondrial variability leads to a large increase in the total noise in mRNA expression levels: without extrinsic factors, the noise in mRNA expression at a given time ($t = 8.3$ hours) was $\eta_m \simeq 0.10$, whereas $\eta_m \simeq 0.40$ with extrinsic factors.

We can also perform simulations on the more complicated system involving protein production (see ‘mRNA & Protein Levels’ in Supplementary Information). With values from Raj *et al.* [15] for protein degradation and translation rate (see Methods), this approach allows us to simulate dual reporter experiments, where the expression of two distinct but identically regulated

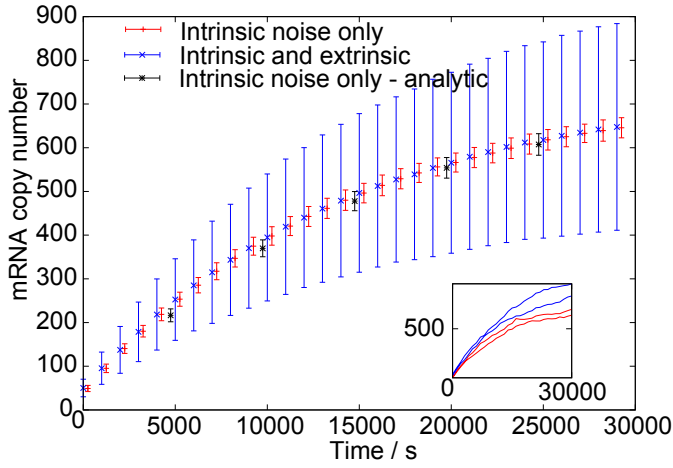


Figure 5: **Extrinsic noise contributes strongly to mRNA level variability.** Analytic and modified Gillespie simulation results for time evolution of mRNA levels with and without mitochondrial and volume variability. Thick lines give the mean value of the corresponding distribution, and analytic results closely match this value but are omitted for clarity. Red (+) give simulated results without inherited variability. Black (*) give analytic results without inherited variability. Blue (x) give simulated results with mitochondrial and volume variability. The inset shows two example time series for both simulated cases.

protein-encoding genes is measured. Each protein was translated from a different mRNA strand, so these simulations tracked four quantities: the expression levels of the two mRNAs and the two proteins. Simulations were performed on synchronised and asynchronous cells, and with σ_n, σ_f set to their model values and set to zero. In these simulations, mRNA molecules and proteins were also distributed binomially between daughter cells at mitosis (see Methods).

Dual reporter simulations performed with the parameterisation chosen from Raj *et al.* [15] yield very low values for the magnitude of intrinsic noise. This low intrinsic noise was found to be due to the high copy number of proteins resulting from the parameterisation. To explore noise in systems with lower expression levels, we lowered the copy number of proteins by increasing the rates of mRNA and protein degradation (see Methods). Fig. 6 shows the resulting expression levels in two proteins with and without various sources of extrinsic noise, at the two different degradation rate protocols. These results show that, in our model, mitochondrial variability dominates the noise in protein expression levels. The spread of protein levels with mitochondrial and volume variability is much greater than the two-fold range achieved through cell cycle variability alone. Fig. 6 also illustrates that cells with higher mitochondrial mass and functionality generally have higher protein expression levels, though inheritance noise makes this correlation weaker.

In our model, we find that energy variability arising through mitochondrial stochasticity is the dominant source of variability in transcription rate, mRNA and protein expression levels. However, we note that the causal factors of stochasticity in mRNA and protein levels within the cell are significantly more complicated than the simple transcriptional model presented above. The rates of many of the processes involved in more extended models are functions of many factors which our model does not include. The inclusion of these complicating terms rapidly makes an analytic description of the model impossible. However, we note that stochastic simulation techniques may be used to explore the behaviour of complex model given estimates for the functional dependence of process rates on extrinsic variables [43].

We also note that several studies have observed a decrease in intrinsic noise at higher levels of protein expression [14, 26]. We do observe such a decrease, though in the default parameterisation the magnitude of this effect is very small owing to the consistently low intrinsic noise levels.

Mitochondrial noise, by modulating transcription rate, can affect stem cell differentiation

As an illustrative application of our model, demonstrating its physiological relevance, we consider how, through the extrinsic effects of [ATP] on protein levels, a link between mitochondrial content and stem cell differentiation behaviour may arise. Differentiation dynamics in stem cells have often been modelled as the result of expression asymmetries in lineage regulation genes that interact in a regulatory network [57–60], but the initial sources of this expression variability have not been clearly elucidated and are a topic of active debate. Here we show that transcription rate variability resulting from mitochondrial variability can affect the dynamics of expression of such control genes. Experimentally, a link between stem cell differentiation and mitochondria was suggested by a recent study in mouse embryonic stem cells [36], showing that pluripotent cells with low mitochondrial membrane potential had higher *in vitro* differentiation propensity, whereas those with higher membrane potential remained undifferentiated and formed large teratomas.

We explore two recent models for the cell fate decision between erythroid and myeloid cell fates directed by the cross-antagonistic master lineage regulators GATA1 and PU.1. One model, by Huang *et al.* [61], consists of a coupled ODE system for the expression levels of these two genes, including cross-repression and self-activation term (see Methods). Another model, by Chickarmane *et al.* [62], contains a similar ODE model, expanded to include interactions with a postulated third species which

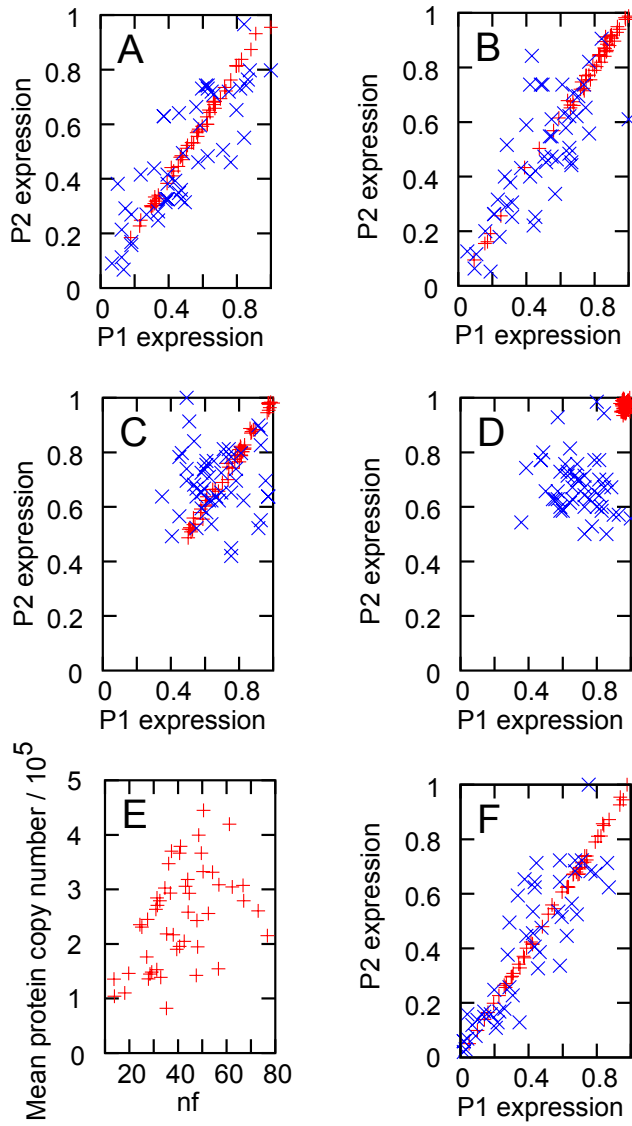


Figure 6: Effects of mitochondrial variability dominate protein expression variability in our model. Dual reporter simulation with different sources of noise in our protein expression simulations. All plots except (E) are normalised so that the highest protein expression level in the cell population is 1. Red (+) show results from Raj *et al.*'s default parameterisation [15] used to model transcription, translation and degradation (see Methods). Blue (x) show results from this parameter set with degradation rates increased 100-fold. Protein levels are shown from population of (A) un-synchronised cells with mitochondrial and volume variability, (B) synchronised cells with mitochondrial and volume variability, (C) un-synchronised cells with no mitochondrial or volume variability, and (D) synchronised cells with no mitochondrial or volume variability. (E) Mean protein expression levels in the default parameterisation of Raj *et al.* with the product of mitochondrial mass and function nf , in the system corresponding to (A). (F) The equivalent plot of (A) with translation rates independent of $[ATP]$.

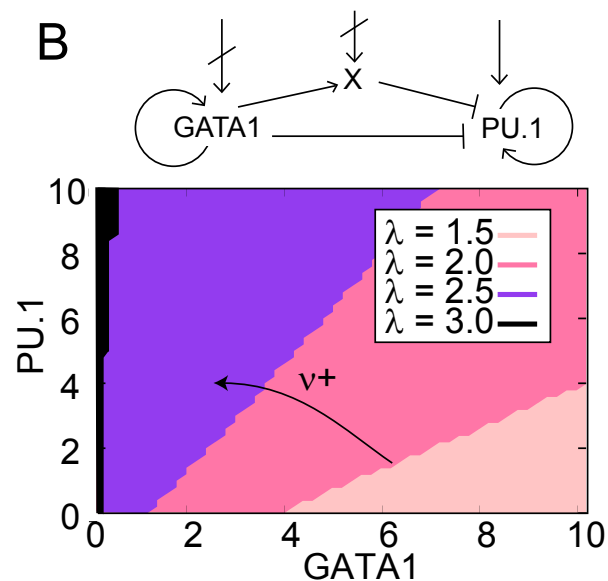
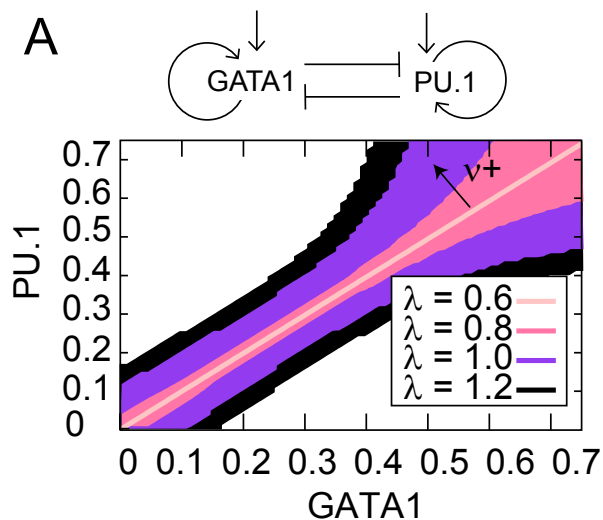


Figure 7: **Transcription rate affects the stability of model stem cell systems.** (A) The structure of the undifferentiated attractor basin in the Huang model given different transcription parameters, showing the widening of the stable undifferentiated region at high transcription rate. (B) The structure of the undifferentiated attractor basin in the Chickarmane model, showing a decrease in undifferentiated basin size as transcription rate increases. The activation-repression structure of both models is illustrated – in (B), external terms representing the activation of GATA1 and X exist but are set to zero in our analysis to allow PU.1 to be expressed under some conditions.

is promoted by GATA1 and represses PU.1. The Chickarmane *et al.* model also includes external signalling terms which may act to promote GATA1 and PU.1, and repress the third species. In these models, cell states are defined by the relative levels of expression of these genes, such that undifferentiated cells have comparable levels of each transcription factor, while the two differentiated cell types correspond to a state with high levels of one factor and low levels of the other. The interactions between the genes are parameterised by variables such as self-activation and cross-repression rates (see Methods). The phase space for both these models comprises three attractor basins, corresponding to the progenitor cell type and two differentiated cell types.

Within the Huang model, at low protein expression levels, smaller perturbations are required to shift attractor basins than at high expression levels – a feature consistent across a large range of parameterisations. Varying the parameterisation of the model (modelling differentiation-inducing signalling) changes the structure of these basins, so that the central undifferentiated basin becomes more or less stable to subsequent perturbation. We vary the default parameterisation of the model in an attempt to assess the effect of changes in transcription and translation rates (see Methods). We find that when the parameters related to the rate of production of proteins are low, the central, undifferentiated state is less stable than when they are high (see Fig. 7A), with a smaller volume of phase space leading to the undifferentiated basin.

Within the Chickarmane model, a different effect is observed. As before, we investigated the volume of phase space corresponding to the basin representing the undifferentiated state. We used a nonzero value for the external signalling term promoting PU.1 and explored the system at different transcription rates (see Methods). We found that increasing the transcription rate led to a decrease in the range of values of the external interaction which supported a stable undifferentiated state (see Fig. 7B). This decrease in the stability of the undifferentiated state arose from a smaller volume of phase space leading to the undifferentiated basin as transcription rate increased, with more phase space occupied by the GATA1 basin. This result contrasts with the increased stability of the Huang model at high transcription rate, due to the importance of the third species (the expression of which is dependent on transcription rate): at high transcription rate, the increased strength of the combined effect of self-activating GATA1 and production of the third species shifts the basin structure strongly towards GATA1.

These results suggest that cell-to-cell variability in mitochondrial mass and function may, through induced variability in transcription rate, have a significant effect on the stability of bipotent cells. If differentiation dynamics are asymmetric and involve an intermediate species (as in the Chickarmane model), we find that high transcription rate destabilises the undifferentiated state, as the combination of a self-activating gene and another species, which both act to repress the competing gene, strongly favours one differentiated basin. If differentiation dynamics are symmetric and do not involve another species (as in the Huang model), high transcription rates increase the width of the basin corresponding to the undifferentiated state, acting to stabilise this state. In both cases, another effect may play a role: several studies have found that, at high protein abundance levels (which may result from high transcription rates), intrinsic noise levels in protein expression decrease. While the parameterisation of our dual reporter studies is such that these effects are small, the fact that less noise is expected at higher protein expression levels suggests a third mechanism by which high mitochondrial content may stabilise pluripotent cells. The contrasting results highlight the potential of experimental investigation of the effects of global transcription rate on the stability of multipotent states to inform of additional qualitative behaviors that models of lineage decision should be expected to exhibit.

Discussion

We have introduced a crude mathematical model for the effects of stochasticity in mitochondrial segregation and functionality on transcription rate in cells. Our model, while simple enough to allow some analytic treatment, reproduces a good number of experimentally observed features concerning the interplay of mitochondrial properties and transcription rate. We analyse our model and find that mitochondria provide extrinsic noise contributions to transcription both through their uneven segregation at mitosis and through variability in their functionality.

We note that, in addition to requiring variability in the amount of mitochondrial mass, an adequate fit to our data required us to consider variability in the function of mitochondria. This connects with the wealth of recent experimental and theoretical interest regarding the causes and control of heterogeneity of mitochondrial function [32, 33, 40, 42] and strengthens the case for the broad physiological relevance of functional variability.

We incorporate our results for mitochondrial-sourced extrinsic noise into existing models for mRNA and protein production, and show that mitochondrial noise can lead to significant variability between cells in a population. We also suggest that transcriptional variability resulting from mitochondrial noise may affect stem cell differentiation, and illustrate this result with an analysis of two recent regulatory network-based models for stem cell differentiation. We find that the quantitative effect of transcription rate variability on stem cell differentiation depends on the architecture of the regulatory network under consideration.

Several recent studies have investigated the interplay between other possible sources of extrinsic noise in various organisms. Before concluding, we will discuss connections to this body of literature. The recent study by Huh and Paulsson [28] found that variability in protein levels due to uneven inheritance at mitosis might explain a body of experimental data that was previously assumed to result from noise in the protein production process. A mathematical study by Rausenberger *et al.* [20] also investigated the effects of inheritance stochasticity on cellular noise. Our work bears significant parallels to these ideas, in that we postulate uneven inheritance of mitochondria to be a substantial contributing factor to noise in all cellular processes that require ATP, including the mechanisms of protein production. Our philosophy also mirrors part of the work of Huh and Paulsson in that our model considers a subset of cellular properties (in our case, mitochondrial partitioning and functionality, and cell volume) to provide all stochastic influences, with all other cellular properties evolving deterministically.

The possible role of ATP as the proxy through which mitochondrial variability affects other cellular processes ties in with an

early prediction of Raser and O’Shea [13] who suggested that the dominance of extrinsic noise in expression variability across a wide range of proteins could result from fluctuations in a factor that affects expression for all genes. ATP, being required for the processes of transcription and translation, meets this criterion. Shahrezaei *et al.* [43] illustrate the fact that extrinsic noise can influence intrinsic noise, through the former’s effects on the rate constants involved in the latter. This influence plays an important role in our model, where extrinsic variability of mitochondrial properties influences the synthesis rates of mRNA and protein through their dependence on $[ATP]$. The ubiquity of ATP as an energy currency within the cell suggests that the rates of other intrinsic processes may be affected by the extrinsic variability we describe.

The link between the process of transcription and noise in protein expression levels that we explore in the last section of this paper is related to the findings of Blake *et al.* [21] who found that protein expression noise depends on transcription efficiency. In our model, the modulation of transcription rate by noisy $[ATP]$ has downstream effects on protein noise levels.

Sigal *et al.* [25], in a study of expression levels over a range of proteins, find cell cycle stage to be a significant contributor to extrinsic noise in protein abundance. Volfson *et al.* [18] used a mathematical framework to similarly identify population dynamics, and upstream transcription factors, as key extrinsic contributors to cellular noise. Our model is compatible with these results, as cells at different cell cycle stages will have had different protein expression histories over their lifetimes. However, we anticipate that mitochondrial variability will also provide a significant contribution to protein expression noise, through modulation of upstream processes.

An in-depth study by Newman *et al.* in yeast cells [14] found a variety of protein-specific differences in expression noise according to transcription mode and protein function. Our model does not capture protein expression noise in this level of detail. The study of Newman *et al.* also characterised the contribution of intrinsic and extrinsic factors to total noise levels as a function of protein abundance. They found that while total expression noise did not scale with protein abundance, noise levels decreased with abundance when extrinsic factors were controlled for: suggesting that extrinsic factors were responsible for maintaining total noise levels as abundance increased. This suggestion that extrinsic noise increases in strength with protein abundance is captured in our protein level simulations.

A study by Bar-Even *et al.*, also in yeast cells [26], found intrinsic noise to be a substantial contributor to total noise, especially for proteins at intermediate abundance levels, with intrinsic contributions becoming less significant as expression levels increase (a similar result to Newman *et al.*). In this and several of the other studies above [14, 21], fluctuations in mRNA number were postulated to be the most important source of noise in protein expression levels. One mRNA molecule may produce many copies of a protein, and regulatory and chromatin-remodelling influences result in stochastic production of mRNA molecules, so random ‘burstiness’ in mRNA levels is a powerful source of noise in protein expression.

Raj *et al.* [15] studied noise in mRNA expression in detail, and identify intrinsic effects as the dominant factors. Their study found that genes located in close proximity to each other displayed synchronised expression, while the expression of genes that were physically separate was unsynchronised, suggesting that local rather than global effects determine the expression levels of genes. While this study demonstrated that intrinsic effects significantly contribute to total noise in some cases, it was not explicitly shown that the magnitude of these effects outweighed extrinsic effects. Our results are compatible with this view that intrinsic noise plays an important role in gene expression, but we suggest that extrinsic noise due to energy variability may also be an important contributor to overall noise levels.

We do not attempt to capture these mRNA processes explicitly: rather, we take transcription rate to be a function of $[ATP]$ as found in experiments [29]. However, we note the result that the measured functional form of this relationship changes in experiments in which chromatin was decondensed. This result suggests that the functional form of transcription rate with $[ATP]$ allows us to capture some effects of the ATP-dependent chromatin remodelling process.

Conclusions

We find, through a phenomenological model constructed to reproduce recent data on mitochondrial and ATP variability, that stochastic inheritance of mitochondria at mitosis and variability in mitochondrial function may be important sources of noise in transcription. By extension, these factors may contribute significantly to noise in protein expression further downstream. We have proposed experimental tests to refine our model and demonstrate its application in existing models for mRNA and protein production and stem cell differentiation, and discussed how these findings integrate into the current understanding of extrinsic noise in cellular biology. In particular, what our paper suggests is the need for multimodal single cell experiments through time (and through division) investigating coarse-grained measures of energy status, cellular volume, mitochondrial mass, and global rates of transcription and translation. Cellular variability is of central physiological importance but we suggest that to understand this we must elucidate the relationships between certain core variables, including the relationship between the machinery of expression and degradation and the energy status of the cell.

Methods

Parameterisation of our model from experimental data. We will use a subset of available experimental data (shown in Fig. 1) to choose numerical values for our key parameters. Henceforth, we will refer to figures in the das Neves *et al.* study [29] as e.g. N1a for Fig. 1a.

We first choose some parameter values for consistency with general cellular properties. As described in ‘Parameterisation of $\lambda(t)$ ’ in Supplementary Information, parameters $s_{1,\dots,4}$, describing the relationship between transcription rate and $[ATP]$, can be found from N2g. For consistency with a recent study [45] on mammalian cell sizes, we choose $v^* = 2500 \mu\text{m}^3$ for the volume at which cells undergo mitosis. Lacking quantitative knowledge of physical quantities relating to mitochondrial functionality, we fix $f_a = 0.5$ and $f_c^0 = 0.5$ to give a mean functionality of 1 in a population of cells.

Parameter	Description	Value	Motivation
f_a	f memory term	0.5	Fit parameter
v^*	Volume for mitosis (scale)	$2\,500\,\mu\text{m}^3$	Fixed for consistency with Ref. [45]
f_c^0	Sets mean functionality (control)	0.5	Fit parameter
γ	Proportionality between $\frac{nf}{v}$ and $[ATP]$	$24\,000\,\mu\text{M}\mu\text{m}^3$	Fixed for consistency with Ref. [53]
α	v growth rate	$0.67\,\text{hr}^{-1}$	Fixed (with β) by known cell cycle length.
β	n growth rate	$0.022\,\text{hr}^{-1}$	Ratio with α fixed by mitochondrial segregation data
σ_v	v standard deviation	$82\,\mu\text{m}^3$	Fixed by volume segregation data
σ_f	f standard deviation	0.3	Constrained by transcription rate noise and cell cycle length variability
$f_c^{(1,-1)}$	Set mean functionality (with anti-oxidant and pro-oxidant respectively)	(0.7, 0.04)	Fixed by transcription rate noise
$s_{1,2,3,4}$	Fitting parameters for relationship between $[ATP]$ and λ	51.2, 44.7, $0.00288\,\mu\text{M}^{-1}$, -1.9	Fixed by functional form of λ (see ‘Parameterisation of $\lambda(t)$ ’ in Supplementary Information)

Table 1: Parameters and values employed in our model.

These choices for mean functionality and maximum cellular volume allow us to use data from das Neves *et al.* [29] to parameterise the distribution of cell volume and mitochondrial mass between sisters at mitosis. Volume segregation data (Fig. 1A, from N4f), given our choice of v^* , allows us to fix a value for the variance in volume inheritance (σ_v in our model). Mitochondrial segregation data (Fig. 1B from N4d), with our assumption of binomial segregation of mitochondria at mitosis, provide us with an estimate of the number of mitochondria in cells undergoing mitosis, which fixes the ratio of β/α in our model. Data on mean cell cycle length (Fig. 1C, from N4h) allows us to fix absolute values of these parameters.

Fixing these values allows us to deduce mean values for mitochondrial mass and cell volume in a population of cells (see next section). Given these quantities, we choose $\gamma = 24\,000\,\mu\text{M}\mu\text{m}^3$ to match experimental data on the mean value of $[ATP]$ in a population of HeLa cells [53].

Parameters relating to the distribution of mitochondrial functionality are less well resolved experimentally. Fixing a value for σ_f involves a tradeoff between our ability to match two experimental observables: the variability of cell cycle lengths (Fig. 1C, from N4h) and the noise in transcription rate in a population of cells (Fig. 1D, from NS12b and NS12d). We used a simple optimisation procedure, described in ‘Fitting Other Parameters’ in Supplementary Information, to fit suitable parameter values for σ_f and the absolute values of α and β to minimise the deviations from experimental data. Given these values, the values of f_c^{-1} and f_c^1 , reflecting changes in mean mitochondrial functionality in the presence of anti-oxidants and pro-oxidants, can be fixed to match the observed noise levels in transcription rate in these situations.

Table 1 summarises the parameters and values employed in our model.

Model Specifics. In the following we provide details of our model. The three equations specifying the key dynamics of v, n and f are respectively Eqns. 1, 2 and 5. The coupling of these variables to transcription rate, $\lambda(n, v, f)$, is through substituting Eqn. 7 into Eqn. 6.

The coupled ODEs in our model admit an analytic solution. Simple integration yields:

$$v(t) = v_0 + \frac{n_0\alpha}{\beta}(\exp(\beta ft) - 1), \quad (1)$$

$$n(t) = n_0 \exp(\beta ft), \quad (2)$$

The reader will note that a variety of models for mitochondrial and volume growth will yield similar forms. In addition, other functional forms for the level of ATP may be suggested. A selection of these alternative forms are explored in ‘Other Models’ in Supplementary Information. Within this model, at mitosis,

$$v_1 = \mathcal{N}\left(\frac{v^*}{2}, \sigma_v\right) \quad (3)$$

$$n_1 = \mathcal{N}\left(\frac{n}{2}, \sqrt{\frac{n}{4}}\right), \quad (4)$$

where $\mathcal{N}(\mu, \sigma)$ is a normal distribution with mean μ and variance σ^2 , and $v_2 = v - v_1, n_2 = n - n_1$ determine the daughter volumes v_1, v_2 and mitochondrial masses n_1, n_2 . The variances of the mitochondrial distribution is chosen to represent a binomial distribution ($\mathcal{B}(n, p) \simeq \mathcal{N}(np, \sqrt{np(1-p)})$, with $p = \frac{1}{2}$, for high n). The variance of the volume distribution is chosen to match experimental data on volume partitioning.

Functionality evolves through changes at mitosis events, which follow an AR(1) process. A daughter cell’s functionality f^D is determined from its parent’s functionality f^P :

$$f^D = f_a f^P + f_c + \mathcal{N}(0, \sigma_f) \quad (5)$$

Upon mitosis, both daughter cells inherit the same f^D value, drawn from Eqn. 10. Once chosen, a cell’s functionality remains constant throughout one cell cycle. We can model treatment with anti- and pro-oxidants by respectively increasing and decreasing f_c , raising or lowering the mean functionality of mitochondria. With $\sigma_f = 0.3$, there is a very small but finite chance that cells will inherit zero (or lower) functionality. To avoid this unphysical case, we impose a cutoff of 0.01 on mitochondrial functionality. Values under this cutoff are resampled from Eqn. 10.

Virtual Mitochondria. In our model, the standard deviation in mitochondrial mass at mitosis is a function of the number of virtual mitochondria in the cell, $\sigma_n = \sqrt{\frac{n}{4}}$, from binomial partitioning. We can vary the number of virtual mitochondria in the cell while keeping the total mitochondrial volume constant, by changing the volume assigned to an individual virtual mitochondrion. Let an individual virtual mitochondria have volume $\frac{v_n}{N}$,

and let there be N virtual mitochondria in a cell. The total mitochondrial volume is v_n , and the mean inherited mitochondrial volume is half of this. The standard deviation in virtual mitochondrial number from a binomial distribution of the virtual mitochondria is $\sqrt{\frac{N}{4}}$, so the standard deviation of mitochondrial volume is $\frac{2v_n}{\sqrt{N}}$. A standard deviation of σ_n then corresponds to $N = \frac{4v_n^2}{\sigma_n^2}$ virtual mitochondria per cell.

Transcription Noise. Transcription rate λ is taken (see ‘Parameterisation of $\lambda(t)$ ’ in Supplementary Information) to be a function of $[ATP]$:

$$\lambda([ATP]) = s_1 + s_2 \tan^{-1}(s_3[ATP] + s_4), \quad (6)$$

and $[ATP] = \frac{\gamma n v}{f}$ can in turn be written in terms of cell age t and cellular initial conditions n_0, v_0, f :

$$[ATP] = \frac{\gamma f n_0 e^{\beta f t}}{v_0 + \frac{n_0 \alpha}{\beta} (e^{\beta f t} - 1)}. \quad (7)$$

If we write σ_t^2 for the variance in observed cellular ages within a population, the variance in $[ATP]$ is given by:

$$\sigma_{[ATP]}^2 = (\partial_{n_0}[ATP])^2 \sigma_{n_0}^2 + (\partial_{v_0}[ATP])^2 \sigma_{v_0}^2 \quad (8)$$

$$+ (\partial_f[ATP])^2 \sigma_f^2 + (\partial_t[ATP])^2 \sigma_t^2, \quad (9)$$

where the individual variances are either known or can be measured from simulation (see ‘Probability Distributions’ and ‘ATP & Transcription Noise’ in Supplementary Information). The variance in transcription rate is then given by

$$\sigma_\lambda^2 = (\partial_{[ATP]}\lambda)^2 \sigma_{[ATP]}^2. \quad (10)$$

If $\eta_i = \frac{\sigma_i}{\mu_i}$ gives the noise level in variable i , the noise in transcription rate, given the parameters used in our model, can be written:

$$\eta_\lambda = \frac{\sigma_\lambda}{\mu_\lambda} = w \sqrt{w_f \eta_f^2 + w_n \eta_n^2 + w_t \eta_t^2 + w_v \eta_v^2}, \quad (11)$$

the quadrature sum of noise in cellular parameters with weighting factors. We find $w_f = 6.2 \times 10^5$, $w_{n_0} = w_{v_0} = 3.1 \times 10^5$, and that w_t is zero within working precision. Typical noise levels in these quantities were measured from simulations as $\eta_f = 0.3$, $\eta_{n_0} = 0.08$, $\eta_{v_0} = 0.06$. These weightings suggest that noise in f is the most dominant contribution to transcriptional noise, followed by noise in n and v , and noise in t (variability in the distribution of cellular ages) is negligible by comparison. The identical weighting for noise levels in n and v still allow n to be the more dominant source of variability, as noise in mitochondrial mass in our model is of a larger magnitude than noise in cellular volumes.

The contribution of mitochondrial stochasticity (n_0 and f) can be found by removing volume segregation noise ($v_0 = 0$) and considering a population of cells at the same point in the cell cycle. We measure cell cycle progression with volume, so fixing $v = v'$ changes the variance in cellular ages σ_t^2 (see ‘ATP & Transcription Noise’ in Supplementary Information).

The noise in transcription rate can be calculated using these variances and expressions for mean $[ATP]$ (using the distribution means of n_0, v_0, f and t) and hence mean λ . Expressions for the transcription rate noise in an unsynchronised population, and the contribution solely due to mitochondrial noise, can then be calculated.

Simulation. To simulate a population of cells, we used a simple Euler method to solve the dynamic equations. A population of $N = 10\,000$ cells was simulated. When mitosis occurred, a random cell from the population was chosen for replacement by the new cell. To measure distributions, this procedure was continued until the distributions stabilised. To measure sister-sister and between-generation correlations, a list of relationships between cells was maintained, with sister pairs only sampled when both sisters underwent an entire cell cycle without replacement.

We note that this removal of randomly-chosen cells may potentially introduce artefacts into the results, as the constant probability of cell removal means that the probability of a cell surviving to a certain age is decreasing. We checked our results with a different simulation protocol: running the system and allowing exponential growth up to 10^6 cells, with no removal. The resulting distributions were indistinguishable from the first protocol, showing that the removal rate is low enough so that the statistics are not affected.

To simulate the master equation systems, we used the modification of Shahrezaei *et al.*’s [43] to the Gillespie simulation method [56]. This extension allows the simulation of time-varying reaction rates into a standard stochastic simulation algorithm. Essentially, each iteration, the simulation calculates whether a reaction or a change of reaction rate will occur first, based on a precompiled table of reaction rates with time. If a reaction occurs first, the population of the system is updated accordingly. If a change in reaction rate occurs first, no reaction is simulated, but the simulation is progressed to the relevant time and reaction rates are updated.

We coupled this simulation protocol with the simple ODE solver so that simulation of a population of cells growing and producing mRNA and protein involved the following algorithm. 1) Use the ODE solver to calculate a cell’s time of mitosis and the time series of volume and transcription rate throughout the cell lifetime. 2) Use Shahrezaei *et al.*’s method to compute the time behaviour of mRNA and protein levels given these time series for production rates. 3) Create daughter cells with noisy partitioning of volume, mitochondrial mass (binomial) and functionality (AR(1)), and mRNA and protein copy numbers (binomial).

After Raj *et al.* [15], we employ the following model values for birth (λ) and death (r) rates of mRNA (m) and protein (n): $\langle \lambda_m \rangle = 0.06 \text{ s}^{-1}$, $\langle \lambda_n \rangle = 0.007 \text{ s}^{-1}$, $r_m = 7 \times 10^{-5} \text{ s}^{-1}$, $r_n = 1.1 \times 10^{-5} \text{ s}^{-1}$. In the case of birth rates, we used these mean values to scale the $\lambda([ATP])$ curves from das Neves *et al.* [29] so that the mean $[ATP]$ level observed in a population gave the mean $\langle \lambda \rangle$ values from Raj *et al.* (see ‘mRNA & Protein Levels’ in Supplementary Information). We also ran experiments with the degradation rates increased 100-fold: $r_m = 7 \times 10^{-3}$, $r_n = 1.1 \times 10^{-3}$, to explore the behaviour of the system at lower expression levels.

Experiments. CMXRos labelling was done according to manufacturer (invitrogen) instructions, cells were incubated with the probe (75 nM) for 15 min. at 37C and washed with warm PBS.

For the dual dye experiments, cells were loaded simultaneously with CMXRos and MitoTracker Green FM dye (Molecular Probes) for 20 min and after a brief PBS rinse fixed in PBS with 4% paraformaldehyde.

Cell cycle length experiments were done by growing cells in the presence of media alone or containing either the anti-oxidant Dithiothreitol (250 microM DTT) or the pro-oxidant Diamide (50 microM). Cell cycle length was measured as the time interval between two mitotic events in a single cell, analysed by live cell imaging using the Cell IQ platform and image analysis software (Chipman Tech.).

In the flow cytometry experiments, trypsinised Hela cells were washed and incubated with 20 nM MitoTracker Green FM dye (Molecular Probes) in medium at 37 C for 15 min, and then washed. Cells were analyzed using flow cytometry (Dako CyAn ADP).

Master equations. Let us consider the master equation for the transcription process:

$$\frac{\partial P_m}{\partial t} = \lambda(t)P_{m-1} + r(m+1)P_{m+1} - (\lambda(t) + rm)P_m, \quad (12)$$

where P_m is the probability of observing m mRNAs at a given time t , $\lambda(t)$ is transcription rate, and r is an mRNA degradation rate.

Using a linear approximation for $\lambda(t)$ (see ‘Parameterisation of $\lambda(t)$ ’ in Supplementary Information), we can solve this (see ‘mRNA & Protein Levels’ in Supplementary Information) to give:

$$P_m(t) = \sum_{i=0}^m \frac{m_0! a_1^i e^{a_2} a_3^{m_0-m+i}}{(m_0-m+i)! i! (m-i)!} \quad (13)$$

where a_1, a_2, a_3 are functions of time and are given in ‘mRNA & Protein Levels’ in Supplementary Information.

Stem Cell Model. The progenitor cell differentiation model of Huang *et al.* [61] consists of the following equations for the evolution of protein expression levels x_1 (GATA1) and x_2 (PU.1):

$$\frac{dx_1}{dt} = a_1 \frac{x_1^n}{\theta_{a1}^n + x_1^n} + b_1 \frac{\theta_{b1}^n}{\theta_{b1}^n + x_2^n} - k_1 x_1 \quad (14)$$

$$\frac{dx_2}{dt} = a_2 \frac{x_2^n}{\theta_{a2}^n + x_2^n} + b_2 \frac{\theta_{b2}^n}{\theta_{b2}^n + x_1^n} - k_2 x_2 \quad (15)$$

In this parameter set, a variables are self-activation rates, b variables are cross-repression rates, k are decay rates, and θ and n control the functional form of these processes. Huang *et al.* show that altering these parameters changes the structure of the corresponding attractor landscape, so that the central undifferentiated attractor basin changes in size, affecting the predisposition of the system to differentiate. This landscape change gives a ‘priming’ of the system such that the effect of subsequent asymmetries may vary. In this study, we vary the landscape by symmetrically varying a and b , the parameters associated with activation and repression, from the default parameterisation $a_i = b_i = k_i = 1, n = 4, \theta_{ai} = \theta_{bi} = 0.5$ for $i = 1, 2$. Specifically, we modulated a and b with a multiplicative factor λ : $a \rightarrow \lambda a, b \rightarrow \lambda b$. We draw the connection between higher values of a and b and higher transcription and translation rates, as the rate of production of chemical species is increased by an increase in these parameters.

The model of Chickarmane *et al.* [62] involves a relationship between three dynamic variables:

$$\frac{d[G]}{dt} = \frac{\alpha_1 A + \alpha_2 [G]}{1 + \beta_1 A + \beta_2 [G] + \beta_3 [G][P]} - \gamma_1 [G] \quad (16)$$

$$\frac{d[P]}{dt} = \frac{\delta_1 B + \delta_2 [P]}{1 + \epsilon_1 B + \epsilon_2 [P] + \epsilon_3 [G][P] + \epsilon_4 [G][X]} - \gamma_2 [P] \quad (17)$$

$$\frac{d[X]}{dt} = \frac{\zeta_1 [G]}{1 + \eta_1 [G] + \eta_2 C} - \gamma_3 [X] \quad (18)$$

where $[G], [P], [X]$ are the concentrations of GATA1, PU.1 and a postulated chemical species X respectively. A, B, C are external signalling factors: A and B promote GATA1 and PU.1 respectively, and C represses X. Other variables take default values $\alpha_1 = \beta_1 = \delta_1 = \epsilon_1 = \beta_3 = \epsilon_3 = 1, \alpha_2 = \beta_2 = \delta_2 = \epsilon_2 = 0.25, \epsilon_4 = 0.13, \gamma_1 = \gamma_2 = \gamma_3 = 0.01, \zeta_1 = \eta_1 = 0.01, \eta_2 = 10$. To vary transcription rates, we modulate α, δ and ζ terms with a multiplicative factor which we take to be proportional to transcription rate λ . We used $B = 0.5$ with $A = C = 0$, allowing an external signal that promotes PU.1, to promote stability of the undifferentiated state.

Acknowledgements

The authors wish to thank Sumeet Agarwal, Maria Domingo-Sananes, Bela Novak and Vahid Shahrezaei for their valuable comments. IGJ and NSJ acknowledge funding from the BBSRC (Grant number: BB/D020190/1), and BG and NSJ acknowledge funding from the EPSRC. FJI has been funded by the Ministerio de Ciencia e Innovacion (Grant number: BFU2009-10792). RpdN is thankful to CNC and MIT-Portugal Program for support.

Supplementary Information

0.1 Parameterisation of $\lambda(t)$

Figs. 2g and 2i in das Neves *et al.* [29] give the response of transcription rate (λ) in arbitrary units to varying concentrations of ATP, without and with artificial decondensation of chromatin respectively. Measuring $[ATP]$ in μM and working with the same arbitrary units employed in that study, we model this response with the expression:

$$\lambda = s_1 + s_2 \tan^{-1}(s_3 [ATP] + s_4), \quad (19)$$

with $s_1 \simeq 51.2, s_2 \simeq 44.7, s_3 \simeq 2.88 \times 10^{-3} \mu M^{-1}, s_4 \simeq -1.9$ (see Fig. 8).

das Neves *et al.* also produced a curve showing λ with $[ATP]$ in an experimental situation involving the decondensation of chromatin in the cell. This curve can be parameterised by the above equation with $s_1^d \simeq 40.0, s_2^d \simeq 54.7, s_3^d \simeq 1.6 \times 10^{-3} \mu M^{-1}, s_4^d \simeq -0.27$.

We choose this inverse tangent functional form to model the response of transcription rate to $[ATP]$ for mathematical simplicity in subsequent sections, and note that modelling with other functional forms (for example, Hill functions) is also possible.

In the parameterisation of our model, the time series of $[ATP]$ in cells is rather linear and slowly varying. This behaviour emerges both due to the dynamics of mitochondrial density (which tends towards $\frac{\beta}{\alpha}$ with time) and the fact that the exponential growths involved are cell-cycle limited to only span a factor of around two before mitosis. It will be useful to employ a linear approximation to $\lambda(t)$, gained from an expansion in t about t' :

$$\lambda(t) = s_1 + s_2 \tan^{-1} \left(s_4 + s_3 \frac{\gamma f n_0 e^{\beta f t}}{v_0 + \frac{n_0 \alpha}{\beta} (e^{\beta f t} - 1)} \right) \quad (20)$$

$$\simeq c + bt, \quad (21)$$

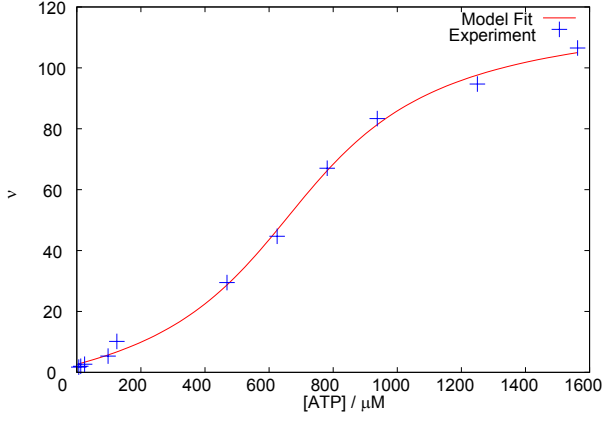


Figure 8: λ with $[ATP]$ (experiment and fit).

where the values of c and b are found after some algebra to be:

$$b = \frac{s_2 f \beta t' \Delta}{(1 + (s_4 + \Delta)^2)} \quad (22)$$

$$c = s_1 + s_2 \tan^{-1}(s_4 + \Delta) - b, \quad (23)$$

and

$$\Delta = \frac{s_3 f n_0 \beta \gamma e^{\beta f t'}}{\alpha n_0 e^{\beta f t'} + \beta v_0 - \alpha n_0}. \quad (24)$$

Constants c and b then depend on cellular initial conditions and t' (which we take to be half the mean cell cycle length) but not on t . The sign of b is determined by the over- or under-population of mitochondria in the cell at mitosis: over-population will lead to high mitochondrial density and mean-reversion will act to decrease transcription rate with time (and *vice versa*).

0.2 Fitting Other Parameters

As described in the Main Text, some parameters in our model were straightforwardly fixed, either for consistency with existing studies on cellular properties (v^* , γ) or to match experimental data from das Neves *et al.* [29] (σ_v). The parameters concerning mitochondrial functionality ($f_a, \sigma_f, f_c^{-1,0,1}$) were less well characterised experimentally. To fix values for these parameters, we first chose values for two parameters (f_a and f_c^0) to give a mean functionality of 1 in the control population, then performed a simple optimisation procedure (see below) to find the values for other parameters. The parameters concerning the growth rates of cell volume and mitochondrial mass (α and β) were also chosen in this optimisation procedure, but initial values were chosen for these parameters, giving suitable results for mean cell cycle length (determined by the magnitude of α and β) and the segregation of virtual mitochondria (determined by the number of mitochondria immediately before mitosis, which is in turn dependent on the ratio of β to α), given a population of cells with uniform functionality.

An optimisation procedure was used to select values for σ_f , α and β . The procedure we used involved choosing random initial conditions for the functionality parameters and initial conditions for the growth rate parameters based on the above constraints, then iterating, choosing a new value for one of the free parameters at each step, and retaining this value if the overall performance of the parameter set improved. The new values were chosen either (with probability 0.1) uniformly from the interval $[0, 2]$ or (with probability 0.9) uniformly from the interval of 10% deviations from the old value. A score for each parameter set was calculated based on the absolute deviation between experimental and simulated observables, averaged over the seven quantities shown in Table 2. Once these values were chosen, $f_c^{-1,1}$ were set to match the experimentally observed transcription noise levels under the corresponding conditions.

We note that although we only used a subset of experimental data to numerically fit the parameters of our model, the model we describe should still be treated with due care. The underlying form of the model was chosen phenomenologically, and from a competing set of alternatives, through a process in which we qualitatively compared model behaviour to the available data from Neves *et al.* [29] – we did not explicitly hide any experimental results when we began the creative process of model construction. Some other possible choices for model forms are described in ‘Other Models’.

0.3 Probability Distributions

0.3.1 Mitochondrial Mass & Cellular Volume

As the dynamics of our model are deterministic, given the initial state of the cell after mitosis, it is instructive to consider the distributions of the descriptive variables during the cell cycle, immediately before and immediately after mitosis. Distributions

Observable	Experimental Value	Simulated Value	Error
η_λ Control	0.4	0.431	0.063
η_λ Anti-oxidant	0.2	0.206	0.032
η_λ Pro-oxidant	1	1.022	0.022
η_λ Sister Cells	0.08	0.089	0.118
SD n_+/n_-	0.22	0.2	0.1
Cell cycle length	30.5	31.0	0.018
SD cell cycle length	5.16	11.8	1.3

Table 2: Experimental observables and simulated fits obtained through optimisation of fitting parameters.

at arbitrary times can then be constructed.

Imposing mitosis at a cutoff volume v^* ensures that the volume distribution of cells immediately before mitosis is a δ -function centred on v^* . Similarly, the post-mitosis volume distribution is simply the distribution that new volumes are chosen from, $\mathcal{N}\left(\frac{v^*}{2}, \sigma_v\right)$:

$$P_{pre}^v = \delta(v - v^*); \quad (25)$$

$$P_{post}^v = \mathcal{N}\left(\frac{v^*}{2}, \sigma_v\right). \quad (26)$$

The distributions of mitochondrial mass are more complicated. Immediately after mitosis, we have:

$$P_{post}^n(n) = \int dn' P_{pre}^n(n') P_{split}^n(n|n'), \quad (27)$$

where $P_{post}^n(n)$ is the post-mitosis n distribution, $P_{pre}^n(n)$ is the n distribution immediately before mitosis, and $P_{split}^n(n|n')$ is the probability of obtaining a daughter cell with n given a parent with mitochondrial volume n_m at mitosis:

$$P_{split}^n(n|n_m) = \mathcal{N}\left(\frac{n_m}{2}, \sqrt{\frac{n_m}{4}}\right). \quad (28)$$

The pre-mitosis distribution is given by

$$P_{pre}^n(n) = \int df P_f(f) \int dv_0 P_{post}^v(v_0) \int dn_0 P_{post}^n(n_0) P_{evol}(n|f, n_0, v_0), \quad (29)$$

where $P_{evol}(n|f, n_0, v_0)$ is the probability that a cell starting with $\{f, n_0, v_0\}$ will have n at mitosis. Eqn. 29 then arises from integrating the probability of having n at mitosis over all possible $\{f, n_0, v_0\}$ start conditions.

As the model's dynamics are deterministic, P_{evol} takes the form of a δ -function, significantly simplifying matters. The dynamic equations are:

$$n(t) = n_0 \exp(\beta f t); \quad (30)$$

$$v(t) = v_0 + \frac{n_0 \beta}{\alpha} (\exp(\beta f t) - 1). \quad (31)$$

Imposing $v = v^*$ gives the time for mitosis as:

$$t_m = \frac{1}{\beta f} \ln \left(\frac{\beta}{\alpha n_0} (v^* - v_0) + 1 \right), \quad (32)$$

and hence the value of n at mitosis is:

$$n_m(n_0, v_0) = \frac{\beta}{\alpha} (v^* - v_0) + n_0, \quad (33)$$

which we note is independent of f . We can then write, due to the deterministic dynamics:

$$P_{evol}(n|f, n_0, v_0) = P_{evol}(n|n_0, v_0) = \delta(n - n_m(n_0, v_0)). \quad (34)$$

Using

$$\delta(f(x)) = \sum_{i=1}^N \frac{\delta(x - x_i)}{|f'(x_i)|}, \quad (35)$$

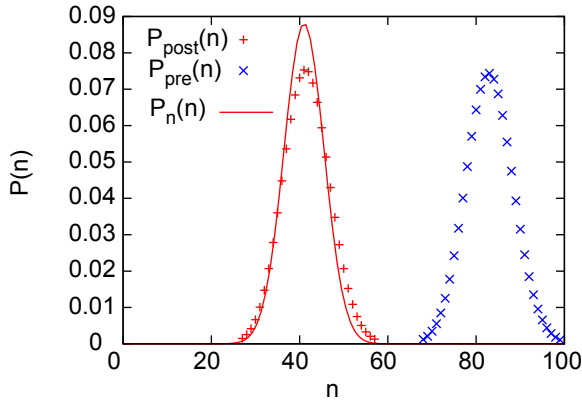


Figure 9: Solutions of Eqn. 37 with $\alpha = 0.67$, $\beta = 0.022$. The solid line shows $P_n(n)$.

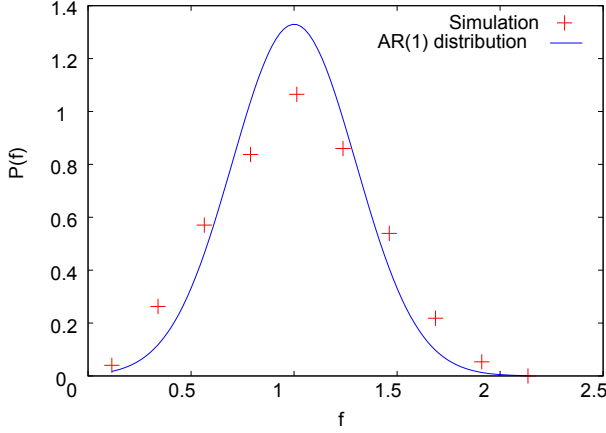


Figure 10: Probability distribution of f under default model parameters, compared to the distribution of the underlying AR(1) process.

where x_i are the roots of $f(x)$, along with the explicit forms of the known probability distributions involved, gives us the following:

$$P_{pre}^n(n) = \int dv_0 (2\pi\sigma_v)^{-\frac{1}{2}} \exp\left(\frac{-(v_0 - \frac{v^*}{2})^2}{2\sigma_v^2}\right) P_{post}^n\left(n - \frac{\beta}{\alpha}(v^* - v_0)\right); \quad (36)$$

$$P_{post}^n(n) = \int dn_m P_{pre}^n(n_m) \left(\frac{\pi n_m}{2}\right)^{-\frac{1}{2}} \exp\left(\frac{-(n - \frac{n_m}{2})^2}{\frac{n_m}{2}}\right). \quad (37)$$

These equations can be numerically solved self-consistently to yield the pre- and post-mitosis n distributions: see Fig. 9. The solution suggests that while the coupling to volume dynamics causes a perturbation to the initial distribution of mitochondrial mass, the approximation $P_{post}(n) \simeq P_{split}\left(n|\frac{\beta}{\alpha}v^*\right)$ will be of use.

The steady-state distribution of the AR(1) process determining f is known to be normal with mean $\frac{f_c}{1-f_a}$ and variance $\frac{\sigma_f^2}{1-f_a^2}$. It is not straightforwardly obvious that the distribution of f in an unsynchronised population of cells, where the lifespan of a cell is a function of f , should also follow this form, but numerical results confirm that the f distribution does closely match it (see Fig. 10).

0.3.2 Cellular Age

The probability of observing a cell in an unsynchronised population, with initial mitochondrial volume n_0 , volume v_0 and functionality f , at time t in its cell cycle is:

$$P(t|t_m(n_0, v_0, f)) = \begin{cases} \frac{1}{t_m} & 0 \leq t \leq t_m; \\ 0 & \text{otherwise.} \end{cases} \quad (38)$$

The probability distribution of t_m in a population of cells is:

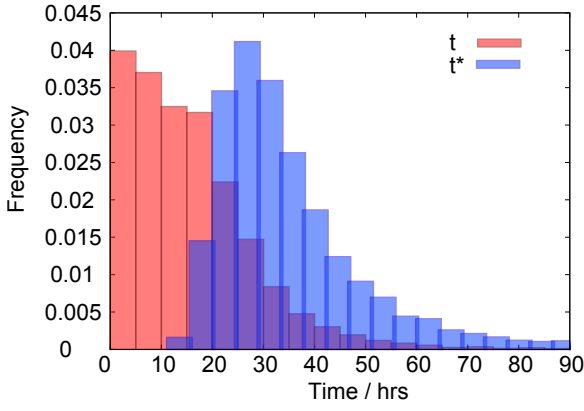


Figure 11: Probability distributions of cellular age t and cell cycle length t^* under default model parameters.

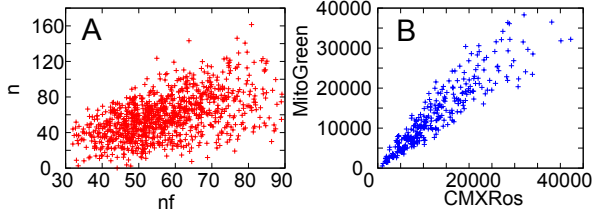


Figure 12: (A) Simulated relationship between a measure of total membrane potential in a cell (the product of mitochondrial mass n and functionality f) and the mitochondrial mass in the cell. (B) Membrane potential (measured with CMXRos) against mitochondrial content (measured with MitoGreen).

$$P(t_m) = \int df \int dn_0 P(n_0, f) \int dv_0 P_v(v_0) \delta \left(t_m - \frac{1}{\beta f} \log \left(\frac{\beta}{n_0 \alpha} (v^* - v_0) + 1 \right) \right), \quad (39)$$

which is difficult to solve. A numeric result is shown in Fig. 11.

It will be useful in further analysis to obtain an approximation for the distribution of cellular ages in an unsynchronised population. This distribution, obtained from simulation, is shown in Fig. 11. The mean and variance of this distribution was found to vary with σ_{n_0} and σ_f , the variance in mitochondrial mass and mitochondrial function. Over the ranges $0 < \sigma_{n_0} < 20$ and $0 < \sigma_f < 0.4$, μ_t varied between 16 and 25 hours and σ_t varied between 9 and 50 hours. However, these terms provide a negligible contribution to the transcription rate variability (we shall show this result in the next section), so we approximate the mean and variance of $P(t)$ to be constant, with $\mu_t \simeq 20.5$ and $\sigma_t \simeq 17$, the values corresponding to the default model parameterisation.

0.4 Mitochondrial Membrane Potential

Fig. 12 shows a comparison of the relationship between total membrane potential in a cell and mitochondrial mass in the cell, from new experiments (see Methods in Main Text) and simulation of our model. Both our model and experimental data shows a linear correlation between total membrane potential and mitochondrial mass. This result emerges straightforwardly from our model due to the representation of total membrane potential (the product of n and f) and the qualitative agreement with experiment suggests that this modelling approach is suitable.

0.5 ATP & Transcription Noise

We have:

$$[ATP] = \frac{\gamma f n}{v} \quad (40)$$

$$= \frac{\gamma f n_0 e^{\beta f t}}{v_0 + \frac{n_0 \alpha}{\beta} (e^{\beta f t} - 1)}, \quad (41)$$

where the second line follows from simple integration of our dynamic equations (Eqns. 1 and 2 in Main Text). From this, the population mean and variance of the ATP distribution can be calculated from the total differential:

$$\mu_{ATP} = \frac{\gamma\mu_f\mu_{n_0}e^{\beta\mu_f\mu_t}}{\mu_{v_0} + \frac{\mu_{n_0}\alpha}{\beta}(e^{\beta\mu_f\mu_t} - 1)}. \quad (42)$$

$$\sigma_{ATP}^2 = \left| \frac{\partial ATP}{\partial n_0} \right|^2 \sigma_{n_0}^2 + \left| \frac{\partial ATP}{\partial f} \right|^2 \sigma_f^2 + \left| \frac{\partial ATP}{\partial v_0} \right|^2 \sigma_{v_0}^2 + \left| \frac{\partial ATP}{\partial t} \right|^2 \sigma_t^2 \quad (43)$$

$$= \frac{e^{2ft\beta}\beta^2\gamma^2}{((e^{ft\beta} - 1)n_0\alpha + v_0\beta)^4} \left(n_0^2 (n_0\alpha (e^{ft\beta} - 1 - ft\beta) + v_0\beta(1 + ft\beta))^2 \sigma_f^2 \right. \\ \left. + f^2 v_0^2 \beta^2 \sigma_{n_0}^2 + f^4 n_0^2 \beta^2 (n_0\alpha - v_0\beta)^2 \sigma_t^2 + f^2 n_0^2 \beta^2 \sigma_{v_0}^2 \right) \quad (44)$$

$$= W_{n_0}^2 \sigma_{n_0}^2 + W_{v_0}^2 \sigma_{v_0}^2 + W_t^2 \sigma_t^2 + W_f^2 \sigma_f^2. \quad (45)$$

Here, μ_{v_0} and σ_{v_0} are known from the post-mitosis distribution of volume, being fundamental parameters in our model. μ_{n_0} and σ_{n_0} can be approximated by the distribution shown in Fig. 9, which was found in ‘Probability Distributions’ to be a good estimate of the simulated mitochondrial distribution at birth. μ_f and σ_f can similarly be approximated as described in Section 0.3. μ_t and σ_t can be measured from the distribution of cellular ages in a population of unsynchronised cells, as in ‘Probability Distributions’. In the last line, all constants have been absorbed into weighting factors W which give the coefficients of the variances of each factor in the full expression for σ_{ATP}^2 . We can then calculate the mean and variance of the distribution of $[ATP]$ in a population.

As transcription rate λ depends solely on $[ATP]$ in our model, we can then calculate the mean and variance of the distribution of λ :

$$\mu_\lambda = s_1 + s_2 \tan^{-1}(s_3 \mu_{ATP} + s_4) \quad (46)$$

$$\sigma_\lambda^2 = \left| \frac{\partial \lambda}{\partial ATP} \right|^2 \sigma_{ATP}^2 \quad (47)$$

$$= \left(\frac{s_2 s_3 \sigma_{ATP}}{1 + (\mu_{ATP} s_3 + s_4)^2} \right)^2. \quad (48)$$

From this, we can explore the contributions of mitochondrial segregation ($\sigma_{n_0}^2$) and functional diversity (σ_f^2) on transcription rate noise $\eta_\lambda = \frac{\sigma_\lambda}{\mu_\lambda}$. The overall expression can be written:

$$\eta_\lambda = \frac{\sigma_\lambda}{\mu_\lambda} \quad (49)$$

$$= \frac{s_2 s_3 \sigma_{ATP}}{(s_1 + s_2 \tan^{-1}(s_3 \mu_{ATP} + s_4))(1 + (\mu_{ATP} s_3 + s_4)^2)} \quad (50)$$

$$= \frac{s_2 s_3 \sqrt{W_{n_0}^2 \sigma_{n_0}^2 + W_{v_0}^2 \sigma_{v_0}^2 + W_t^2 \sigma_t^2 + W_f^2 \sigma_f^2}}{(s_1 + s_2 \tan^{-1}(s_3 \mu_{ATP} + s_4))(1 + (\mu_{ATP} s_3 + s_4)^2)} \quad (51)$$

$$= w \sqrt{w_f \eta_f^2 + w_{n_0} \eta_{n_0}^2 + w_t \eta_t^2 + w_{v_0} \eta_{v_0}}, \quad (52)$$

where the last line condenses the expression into the quadrature sum of noise levels in cellular parameters with weighting factors $w_i = W_i^2 \mu_i^2$. We find, with our default parameter set, $w_f = 6.2 \times 10^5$, $w_{n_0} = w_{v_0} = 3.1 \times 10^5$, and that w_t is zero within working precision. Typical noise levels in these quantities were measured from simulations as $\eta_f = 0.3$, $\eta_{n_0} = 0.08$, $\eta_{v_0} = 0.06$.

0.6 Other Models

0.6.1 ATP and Alternatives

It is thought that ATP levels in the cell are subject to homeostasis. For this reason we do not include a sink term for ATP, assuming that an ATP deficit will be immediately compensated for. A model that would capture ATP usage is given by:

$$\dot{v} = \alpha' \frac{a}{v} \quad (53)$$

$$\dot{n} = \beta' \frac{a}{v} \quad (54)$$

$$\dot{a} = \gamma' n - (\alpha' + \beta') \frac{a}{v}, \quad (55)$$

where a is the cellular ATP level. Here, the second term in Eqn. 55 corresponds to the rate of use of ATP in increasing the cell volume and mitochondrial mass. Note that if $a = \gamma n$ our model equations are recovered. This model, with a suitable parameterisation, produces very similar results to our simpler model.

Label	Equations	Description
A	$\dot{v} = \alpha n$ $\dot{n} = \beta n$	Default model type
B	$\dot{v} = \alpha v$ $\dot{n} = \beta v$	Volume control on growth
C	$\dot{v} = \alpha n$ $\dot{n} = \alpha n \left(\gamma - \frac{n}{v} \right)$	Strong, explicit mean reversion of n towards a density γ .
D	$\dot{v} = \alpha v \left(1 - \frac{v}{v^*} \right)$ $\dot{n} = \alpha n \left(\gamma - \frac{n}{v} \right)$	Explicit mean reversion of n towards γ , and volume growth towards a target v^*
E	$\dot{v} = \alpha$ $\dot{n} = \beta n \left(\gamma - \frac{n}{v} \right)$	Linear volume growth
F	$\dot{v} = \alpha$ $\dot{n} = \beta \left(\gamma - \frac{n}{v} \right)$	Linear volume growth and weaker mean reversion on n

Table 3: Different possible models for time evolution of the cell exhibiting mean reversion. Each of these expressions admits an analytic solution for $n(t)$ and $v(t)$. Other combinations (for example, weak mean reversion on n and exponential volume growth) are harder to solve and are often unstable for high or low initial n/v .

We also note that the following system explicitly incorporates ATP homeostasis, as ATP is produced up to a certain level by mitochondria and used up in the increase of cellular volume:

$$\dot{a} = k^+(a^* - a)n - k^-av, \quad (56)$$

where a^* controls the homeostatic level of ATP. This equation is solved by

$$a = a_0 e^{-t(k^+n - k^-v)} + \frac{a^*k^+n}{k^+n + k^-v}, \quad (57)$$

giving a hyperbolic form for ATP levels in terms of n and v . This representation could easily be extended to allow consideration of the ATP:ADP ratio – in which the rate of use of ATP gives the rate of production of ADP and vice versa.

It is also possible that ROS plays a role in modulating transcription rate and cellular growth rates. In this case, an additional term could be introduced into the model, proportional to the number of mitochondria, and possibly inversely proportional to mitochondrial functionality, and used to modulate the dynamic equations and transcription rate.

In our current model, we do not consider these complicating factors, due to our lack of experimental justification for them and also due to our desire to retain a simple, analytically tractable model. Future work, possibly motivated by the experiments we suggest in the main text, could take these more complicated factors into account.

0.6.2 Other Dynamic Forms

Our model has been chosen phenomenologically to match experimental results concerning the distribution and behaviour of mitochondria. Other models are possible that display similar behaviour. Here we mention some potential alternative models. These alternatives both incorporate mean reversion on mitochondrial density and yield sensible key results. There is a difference in mean reversion rate between these models, illustrated by dynamic plots in Fig. 13.

Our model was chosen for its analytic tractability and its ability to reproduce experimental phenomena: these more complex models rapidly become analytically intractable, which hinders a deeper understanding of their behaviour.

We note in addition that the $[ATP]$ term that appears in our dynamic equations may be replaced by a transcription or translation rate term, explicitly including the sigmoidal (or hyperbolic) response of these cellular growth rates in the dynamic equations. In our bare model, we use the simpler $[ATP]$ term both to maintain analytic tractability and because the appropriate form for a response curve is difficult to estimate (for example, cellular growth may be a result of a combination of transcription and translation, and may include other additional terms). This approach essentially involves using a linear approximation for growth rate: linear approximations for transcription rate are employed elsewhere in this study and yield very similar results to the numerical behaviour of the corresponding nonlinear case.

It is possible to construct models for mitochondrial stochasticity that do not involve mean-reverting behaviour of mitochondrial density. As a simple example, if cellular dynamics are such that mitochondrial mass and cellular volume evolve independently:

$$\dot{v} = \alpha f v; \quad (58)$$

$$\dot{n} = \beta f n, \quad (59)$$

with mitosis involving a binomial segregation of volume and mitochondrial mass as before, the population variance in mitochondrial density will generally increase in an unbounded manner, as the probability of observing higher and higher mitochondrial

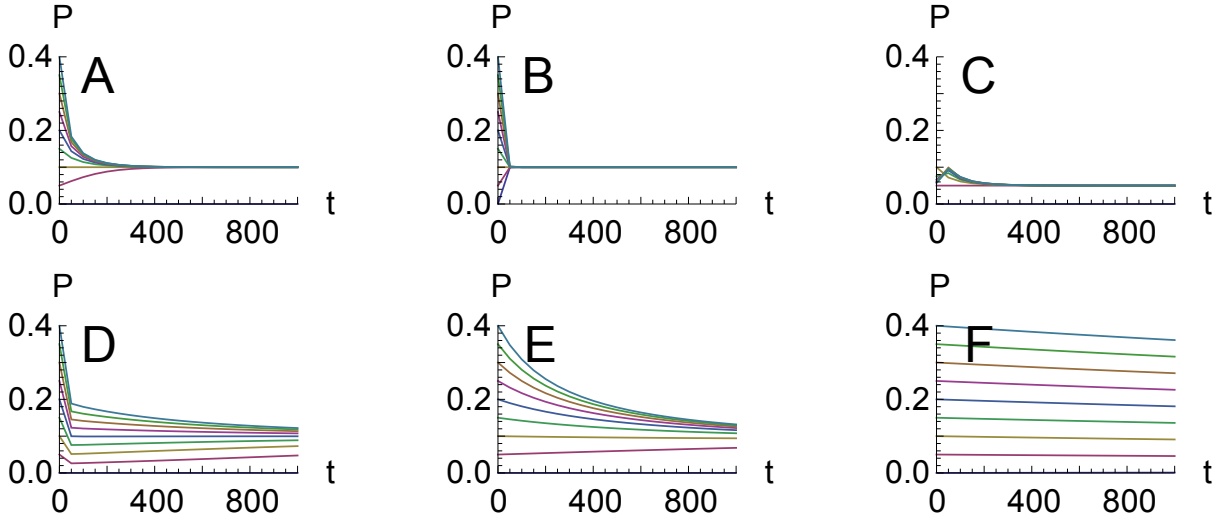


Figure 13: The functional form of mitochondrial density ρ with time t (in arbitrary units) in other possible models for the time evolution of cellular properties. For these illustrations, the parameter set $\alpha = 0.1, \beta = 0.01, v_0 = 1000$ is used. The different lines correspond to trajectories of ρ resulting from varying initial n_0 between 0 and 400 (a much wider range than in the default model, as different choices of functional form may lead to different absolute values for n and v). The label of the plot gives the corresponding function in Table 3.

densities increases with time. However, if cutoffs are placed on mitochondrial density, so that cells are removed from the population if their density does not obey

$$\rho_- < \frac{n}{v} < \rho_+, \quad (60)$$

the population distribution of mitochondrial density can achieve stationarity. This approach results in a much weaker correlation between mitochondrial mass n and cellular volume v . This model can be parameterised (an example parameter set is $\rho_- = 10, \rho_+ = 300, \alpha = \beta = 0.1, \gamma = 3.6$, other parameters the same as in the default model) to yield similar results to the default model for transcriptional noise.

Obtaining analytic results from this model is difficult, both in terms of approximation for the moments of probability distributions and the time evolution of mRNA.

This rather constructed model is considered due to the discrepancy between flow cytometry data in das Neves *et al.* [29], showing an absence of correlation between mitochondrial volume and cellular volume.

0.7 Potential Experiments for Refinement

As mentioned in the Main Text, our model was constructed from a phenomenological philosophy, with the intention of using experimental results to construct a plausible coarse-grained explanation for the influence of mitochondrial variability on extrinsic noise in general and transcription rate in particular. Our goal was to introduce a simplified but consistent mathematical summary of the data and to use this to motivate further experiments. We suggest a set of experiments in Table II that would support or contribute to further development of this model.

0.8 mRNA & Protein Levels

The master equation for the probability distribution of mRNA levels can be written down as:

$$\frac{\partial P_m}{\partial t} = \lambda(t)P_{m-1} + r(m+1)P_{m+1} - (\lambda(t) + rm)P_m, \quad (61)$$

where $\lambda(t)$ is the time-dependent birth rate of mRNA molecules, r is the rate of removal of mRNA, and $P_m(t)$ is the probability of observing the system with m mRNA molecules at time t . We choose

$$\lambda(t) = (c + bt), \quad (62)$$

the approximation from ‘Parameterisation of $\lambda(t)$ ’, to model transcription rate with time.

Using the generating function $G(z) = \sum_m z^m P_m$ gives:

$$\frac{\partial G}{\partial t} = \lambda(t)(z-1)G - r(z-1)\frac{\partial G}{\partial z}. \quad (63)$$

	Observable	Prediction
1	Mitochondrial functionality (measured via membrane potential) before and after mitosis.	Parent membrane potential is weakly retained but stochastically altered to give daughter membrane potential.
2	Protein expression levels as a function of $[ATP]$.	Expression levels are higher in cells with higher $[ATP]$.
3	Time series of mitochondrial mass and density through the cell cycle..	Exponential cell growth, with mitochondrial density tending towards an average value. The time series of these dynamics could be used to distinguish between different models (see ‘Other Models’).
4	Behaviour of $[ATP]$ with time.	Slowly varying over the cell cycle, mean-reverting towards an average value.
5	Determinant factors of $[ATP]$.	Mitochondrial mass and membrane potential, and cell volume. Levels of ROS may also be of importance.
6	Relative contribution of mitochondrial mass and functional variability to transcriptional variability (measured via bromouridine uptake).	Strong dependence of transcriptional noise on both mitochondrial inheritance and functionality variability.
7	Noise in protein expression levels.	Dependent on mitochondrial variability, and lower for cells with mitochondrial low mass and functionality.
8	ROS levels (measured via, for example, MitoSox).	Possibly correlated inversely with a measure of mitochondrial functionality, and possibly higher with low mitochondrial mass and functionality, as weaker/sparser mitochondria struggle to match energy demands.

Table 4: Potential experiments that may clarify aspects of our model, roughly ranked in order of importance for supporting or suggesting area of refinement for our model.

We can solve Eqn. 63 with the method of characteristics. This process allows us to convert the PDE into a set of ODEs along a characteristic curve of the function. We wish to recast Eqn. 63 into the following form, where a characteristic curve is parameterised by the new variable s :

$$\frac{d}{ds}G(z(s), t(s)) = F(G, z(s), t(s)). \quad (64)$$

Using the chain rule, we can write:

$$\frac{d}{ds}G(z(s), t(s)) = \frac{\partial G}{\partial z} \frac{dz}{ds} + \frac{\partial G}{\partial t} \frac{dt}{ds} \quad (65)$$

$$= \frac{1}{z-1} \frac{\partial G}{\partial t} + r \frac{\partial G}{\partial z} = (c + bt)G, \quad (66)$$

where the last line is just a rearrangement of the original PDE. By comparing coefficients, we have:

$$\frac{dz}{ds} = r, z = rs + c_1 \quad (67)$$

$$\frac{dt}{ds} = \frac{1}{z-1} = \frac{1}{rs + c_1 - 1}, t = \frac{1}{r} \ln(rs + c_1 - 1) + c_2, \quad (68)$$

$$\frac{dG}{ds} = (c + bt)G = \left(c + b \left(\frac{1}{r} \ln(rs + c_1 - 1) + c_2 \right) \right) G. \quad (69)$$

As absolute values of s are not important, affecting only the parameterisation of progress along a characteristic curve, we set $c_1 = 0$. The final ODE can then be solved by separation of variables:

$$\int \frac{1}{G} dG = \int \left(c + b \left(\frac{1}{r} \ln(rs + c_1 - 1) + c_2 \right) \right) ds \quad (70)$$

$$= s(c + bc_2) - \frac{sb}{r} + \frac{sb}{r} \ln(rs - 1) - \frac{b}{r^2} \ln(rs - 1) \quad (71)$$

$$= \frac{z}{r}(c + bt) - \frac{bz}{r^2} - \frac{b}{r^2} \ln(z - 1), \quad (72)$$

where the final line follows from $s = \frac{z}{r}$ and $c_2 = t - \frac{1}{r} \ln(z - 1)$. We then have

$$G = \exp \left(\frac{z}{r}(c + bt) - \frac{bz}{r^2} \right) (z - 1)^{-\frac{b}{r^2}} c_3, \quad (73)$$

where the arbitrary function $c_3 = c_3(t - \frac{1}{r} \ln(z-1)) = c_3(c_2)$, as this quantity is independent of s .

If the initial copy number of mRNA molecules is m_0 , we have the initial condition $G(z, 0) = \sum_m z^m P_m(0) = \sum_m z^m \delta_{m m_0} = z^{m_0}$. Noting that at $t = 0$, $e^{-c_2 r} = z - 1$, we find that if we employ the choice

$$c_3(c_2) = \exp \left((e^{-c_2 r} + 1) \left(\frac{b}{r^2} - \frac{c}{r} \right) \right) (e^{-c_2 r} + 1)^{m_0} \exp \left(\frac{-b}{r^2} c_2 r \right), \quad (74)$$

we recover the required initial condition:

$$G(z, t) = \exp \left(\frac{z}{r} (c + bt) - \frac{bz}{r^2} \right) (z-1)^{\frac{-b}{r^2}} \exp \left((e^{-c_2 r} + 1) \left(\frac{b}{r^2} - \frac{c}{r} \right) \right) (e^{-c_2 r} + 1)^{m_0} \exp \left(\frac{-b}{r^2} c_2 r \right) \quad (75)$$

$$G(z, 0) = \exp \left(\frac{zc}{r} - \frac{bz}{r^2} \right) (z-1)^{\frac{-b}{r^2}} \exp \left(z \left(\frac{b}{r^2} - \frac{c}{r} \right) \right) z^{m_0} (z-1)^{\frac{b}{r^2}} \quad (76)$$

$$= z^{m_0}. \quad (77)$$

The general solution is then:

$$G(z, t) = \exp \left(\frac{z}{r} (c + bt) - \frac{bz}{r^2} \right) (z-1)^{\frac{-b}{r^2}} \exp \left((e^{-c_2 r} + 1) \left(\frac{b}{r^2} - \frac{c}{r} \right) \right) (e^{-c_2 r} + 1)^{m_0} \exp \left(\frac{-b}{r^2} c_2 r \right) \quad (78)$$

$$= \exp \left(\frac{1}{r} \left(z \left(c + bt - \frac{b}{r} \right) - \left(c + bt - \frac{b}{r} \right) \right) + \frac{(z-1)e^{-rt}}{r} \left(\frac{b}{r} - c \right) - rtm_0 \right) \quad (79)$$

$$\times (z-1)^{\frac{b}{r^2} - \frac{b}{r^2}} (z + e^{rt} - 1)^{m_0} \quad (79)$$

$$= e^{a_1 z + a_2} (z + a_3)^{m_0}, \quad (80)$$

with

$$a_1 = \frac{1}{r} \left(c + bt - ce^{-rt} - \frac{b}{r} + \frac{be^{-rt}}{r} \right) \quad (81)$$

$$a_2 = -m_0 tr - a_1 \quad (82)$$

$$a_3 = e^{rt} - 1 \quad (83)$$

We recover the probability of observing m mRNAs using $P_m(t) = \frac{1}{m!} \frac{\partial^m G}{\partial z^m} \Big|_{z=0}$. Using Leibniz's rule allows us to write:

$$P_m(t) = \frac{1}{m!} \frac{\partial^m G}{\partial z^m} \Big|_{z=0} \quad (84)$$

$$= \frac{1}{m!} \sum_{i=0}^m \binom{m}{i} \frac{\partial^i}{\partial z^i} e^{a_1 z + a_2} \frac{\partial^{m-i}}{\partial z^{m-i}} (z + a_3)^{m_0} \Big|_{z=0} \quad (85)$$

$$= \sum_{i=0}^m \frac{1}{i!(m-i)!} a_1^i e^{a_1 z + a_2} \frac{m_0!}{(m_0 - m + i)!} (z + a_3)^{m_0 - m + i} \Big|_{z=0} \quad (86)$$

$$= \sum_{i=0}^m \frac{m_0! a_1^i e^{a_2} a_3^{m_0 - m + i}}{(m_0 - m + i)! i! (m-i)!}. \quad (87)$$

The corresponding master equation including proteins is:

$$\begin{aligned} \frac{\partial P_{m,n}}{\partial t} &= m\lambda_n(t)P_{m,n-1} + r_n(n+1)P_{m,n+1} - r_n n P_{m,n} - m\lambda_n(t)P_{m,n} \\ &+ \lambda_m(t)P_{m-1,n} + r_m(m+1)P_{m+1,n} - r_m m P_{m,n} - \lambda_m(t)P_{m,n}. \end{aligned} \quad (88)$$

To simulate these systems, we use a parameter set employed by Raj *et al.* [15]: $\langle \lambda_m \rangle = 0.06 s^{-1}$, $\langle \lambda_n \rangle = 0.007 s^{-1}$, $r_m = 7 \times 10^{-5} s^{-1}$, $r_n = 1.1 \times 10^{-5} s^{-1}$. The death rates are simply inserted into the simulation, and the mean birth rates are used to tune the time-varying birth rate for the simulation. For example, the normalisation of $\lambda_m(t)$ was chosen so that the mean value of $[ATP]$ (see 'ATP & Transcription Noise') corresponded to $\langle \lambda_m \rangle$.

As the process of translation is believed to be $[ATP]$ -dependent but not dependent on chromatin remodelling, the decondensed version of Eqn. 19 (using the hyperbolic s_i^d coefficients rather than the sigmoidal s_i coefficients) was used for λ_n . Again, the mean birth rate was used to normalise this function as above. Overall, we then have constant rates for mRNA death (faster) and protein death (slower) and time-varying birth rates for mRNA (including chromatin remodelling) and proteins (not including chromatin remodelling).

As mentioned in the Main Text, we found this parameterisation to yield large copy numbers of proteins, which led to very low values for intrinsic noise. We explored this effect by increasing the degradation rates from Raj *et al.*'s default values, to $r_m = 7 \times 10^{-3} s^{-1}$, $r_n = 1.1 \times 10^{-3}$. In addition, we investigated the case where variability in $[ATP]$ only affected transcription rate, with translation rate taking the constant value $\lambda_n = 0.007 s^{-1}$. As shown in the Main Text, those simulations with higher degradation rates showed a more significant intrinsic noise contribution, and the trends in these dual reporter simulations changed little with a constant translation rate. This consistency means that though our crude model of the dependence of translation rate on $[ATP]$ could be challenged, even if translation is ATP dependent we still see pronounced effects on protein levels through ATP-dependent variability in transcription rate.

References

1. McAdams HH, Arkin A (1997) Stochastic mechanisms in gene expression. *Proc Natl Acad Sci USA* 94: 814–819.
2. Altschuler S, Wu L (2010) Cellular Heterogeneity: Do Differences Make a Difference? *Cell* 141: 559–563.
3. Elowitz MB, Levine AJ, Siggia ED, Swain PS (2002) Stochastic gene expression in a single cell. *Science* 297: 1183–1186.
4. Kærn M, Elston TC, Blake WJ, Collins JJ (2005) Stochasticity in gene expression: from theories to phenotypes. *Nat Rev Genet* 6: 451–464.
5. Raj A, van Oudenaarden A (2008) Nature, nurture, or chance: stochastic gene expression and its consequences. *Cell* 135: 216–226.
6. Chang H, Hemberg M, Barahona M, Ingber D, Huang S (2008) Transcriptome-wide noise controls lineage choice in mammalian progenitor cells. *Nature* 453: 544–547.
7. Fraser D, Kærn M (2009) A chance at survival: gene expression noise and phenotypic diversification strategies. *Mol Microbiol* 71: 1333–1340.
8. Kussell E, Kishony R, Balaban N, Leibler S (2005) Bacterial persistence: a model of survival in changing environments. *Genetics* 169: 1807.
9. Brock A, Chang H, Huang S (2009) Non-genetic heterogeneity – a mutation-independent driving force for the somatic evolution of tumours. *Nat Rev Genet* 10: 336–342.
10. Bastiaens P (2009) Systems biology: when it is time to die. *Nature* 459: 334–335.
11. Spencer S, Gaudet S, Albeck J, Burke J, Sorger P (2009) Non-genetic origins of cell-to-cell variability in TRAIL-induced apoptosis. *Nature* 459: 428–432.
12. Swain P, Elowitz M, Siggia E (2002) Intrinsic and extrinsic contributions to stochasticity in gene expression. *Proc Natl Acad Sci USA* 99: 12795.
13. Raser JM, O'Shea EK (2004) Control of stochasticity in eukaryotic gene expression. *Science* 304: 1811–1814.
14. Newman JRS, Ghaemmaghami S, Ihmels J, Breslow DK, Noble M, et al. (2006) Single-cell proteomic analysis of *S. cerevisiae* reveals the architecture of biological noise. *Nature* 441: 840–846.
15. Raj A, Peskin CS, Tranchina D, Vargas DY, Tyagi S (2006) Stochastic mRNA synthesis in mammalian cells. *PLoS Biol* 4: e309.
16. Paulsson J (2005) Models of stochastic gene expression. *Phys Life Rev* 2: 157–175.
17. Paulsson J (2004) Summing up the noise in gene networks. *Nature* 427: 415–418.
18. Volfson D, Marciniak J, Blake WJ, Ostroff N, Tsimring LS, et al. (2005) Origins of extrinsic variability in eukaryotic gene expression. *Nature* 439: 861–864.
19. Bruggeman F, Blüthgen N, Westerhoff H (2009) Noise management by molecular networks. *PLoS Comp Biol* 5: 1183–1186.
20. Rausenberger J, Kollmann M (2008) Quantifying origins of cell-to-cell variations in gene expression. *Biophys J* 95: 4523–4528.
21. Blake WJ, Kærn M, Cantor CR, Collins JJ (2003) Noise in eukaryotic gene expression. *Nature* 422: 633–637.
22. Dobrzyński M, Bruggeman FJ (2009) Elongation dynamics shape bursty transcription and translation. *Proc Natl Acad Sci USA* 106: 2583–2588.
23. Thattai M, Van Oudenaarden A (2001) Intrinsic noise in gene regulatory networks. *Proc Natl Acad Sci USA* 98: 8614.

24. Sigal A, Milo R, Cohen A, Geva-Zatorsky N, Klein Y, et al. (2006) Variability and memory of protein levels in human cells. *Nature* 444: 643–646.
25. Sigal A, Milo R, Cohen A, Geva-Zatorsky N, Klein Y, et al. (2006) Dynamic proteomics in individual human cells uncovers widespread cell-cycle dependence of nuclear proteins. *Nature Methods* 3: 525–531.
26. Bar-Even A, Paulsson J, Maheshri N, Carmi M, O'Shea E, et al. (2006) Noise in protein expression scales with natural protein abundance. *Nature Genetics* 38: 636–643.
27. Kaufmann B, van Oudenaarden A (2007) Stochastic gene expression: from single molecules to the proteome. *Curr Opin Gen Dev* 17: 107–112.
28. Huh D, Paulsson J (2010) Non-genetic heterogeneity from stochastic partitioning at cell division. *Nat Genetics* 43: 95–102.
29. das Neves RP, Jones NS, Andreu L, Gupta R, Enver T, et al. (2010) Connecting Variability in Global Transcription Rate to Mitochondrial Variability. *PLoS Biol* 8: 451–464.
30. McBride H, Neuspiel M, Wasiak S (2006) Mitochondria: more than just a powerhouse. *Curr Biol* 16: R551–R560.
31. Chan D (2006) Mitochondria: dynamic organelles in disease, aging, and development. *Cell* 125: 1241–1252.
32. Twig G, Hyde B, Shirihai O (2008) Mitochondrial fusion, fission and autophagy as a quality control axis: the bioenergetic view. *BBA — Bioenergetics* 1777: 1092–1097.
33. Collins TJ, Berridge MJ, Lipp P, Bootman MD (2002) Mitochondria are morphologically and functionally heterogeneous within cells. *EMBO J* 21: 1616–1627.
34. Buckman JF, Reynolds IJ (2001) Spontaneous changes in mitochondrial membrane potential in cultured neurons. *J Neurosci* 21: 5054–5065.
35. O'Reilly CM, Fogarty KE, Drummond RM, Tuft RA, Walsh JV (2003) Quantitative analysis of spontaneous mitochondrial depolarizations. *Biophys J* 85: 3350–3357.
36. Schieke SM, Ma M, Cao L, McCoy JP, Liu C, et al. (2008) Mitochondrial metabolism modulates differentiation and teratoma formation capacity in mouse embryonic stem cells. *J Biol Chem* 283: 28506–28512.
37. Mitra K, Wunder C, Roysam B, Lin G, Lippincott-Schwartz J (2009) A hyperfused mitochondrial state achieved at G1–S regulates cyclin E buildup and entry into S phase. *Proc Natl Acad Sci USA* 106: 11960–11965.
38. Mandal S, Guptan P, Owusu-Ansah E, Banerjee U (2005) Mitochondrial regulation of cell cycle progression during development as revealed by the tenured mutation in *Drosophila*. *Dev Cell* 9: 843–854.
39. Owusu-Ansah E, Yavari A, Mandal S, Banerjee U (2008) Distinct mitochondrial retrograde signals control the G1-S cell cycle checkpoint. *Nat Genet* 40: 356–361.
40. Kuznetsov A, Troppmair J, Sucher R, Hermann M, Saks V, et al. (2006) Mitochondrial subpopulations and heterogeneity revealed by confocal imaging: Possible physiological role? *BBA Bioenergetics* 1757: 686–691.
41. Cossarizza A, Ceccarelli D, Masini A (1996) Functional heterogeneity of an isolated mitochondrial population revealed by cytofluorometric analysis at the single organelle level. *Exp Cell Res* 222: 84–94.
42. Mouli P, Twig G, Shirihai O (2009) Frequency and selectivity of mitochondrial fusion are key to its quality maintenance function. *Biophys J* 96: 3509–3518.
43. Shahrezaei V, Ollivier JF, Swain PS (2008) Colored extrinsic fluctuations and stochastic gene expression. *Molecular Systems Biology* 4: 1–9.
44. Lane N (2006) Mitochondrial disease: powerhouse of disease. *Nature* 440: 600–602.
45. Tzur A, Kafri R, LeBleu VS, Lahav G, Kirschner MW (2009) Cell growth and size homeostasis in proliferating animal cells. *Science* 325: 167–171.
46. Posakony J, England J, Attardi G (1977) Mitochondrial growth and division during the cell cycle in HeLa cells. *J Cell Biol* 74: 468–491.
47. Veltri K, Espiritu M, Singh G (1990) Distinct genomic copy number in mitochondria of different mammalian organs. *J Cell Physiol* 143: 160–164.
48. Herbener G (1976) A morphometric study of age-dependent changes in mitochondrial populations of mouse liver and heart. *J Geront* 31: 8.

49. Mathieu O, Krauer R, Hoppeler H, Gehr P, Lindstedt S, et al. (1981) Design of the mammalian respiratory system. VII. Scaling mitochondrial volume in skeletal muscle to body mass. *Respir Physio* 44: 113–128.
50. Suarez R, Lighton J, Brown G, Mathieu-Costello O (1991) Mitochondrial respiration in hummingbird flight muscles. *Proc Natl Acad Sci USA* 88: 4870.
51. Hoppeler H, Lindstedt S, Claassen H, Taylor C, Mathieu O, et al. (1984) Scaling mitochondrial volume in heart to body mass. *Respir Physio* 55: 131–137.
52. Robin E, Wong R (1988) Mitochondrial DNA molecules and virtual number of mitochondria per cell in mammalian cells. *J Cell Physio* 136: 507–513.
53. Wang R, Tao L, Trumbore M, Berger S (1997) Turnover of the acyl phosphates of human and murine prothymosin α in vivo. *J Biol Chem* 272: 26405.
54. Kumei Y, Nakajima T, Sato A, Kamata N, Enomoto S (1989) Reduction of G1 phase duration and enhancement of c-myc gene expression in HeLa cells at hypergravity. *J Cell Sci* 93: 221–226.
55. Bogenhagen D, Clayton D (1974) The number of mitochondrial deoxyribonucleic acid genomes in mouse L and human HeLa cells. *J Biol Chem* 249: 7991.
56. Gillespie D (1977) Exact stochastic simulation of coupled chemical reactions. *J Phys Chem* 81: 2340–2361.
57. Enver T, Pera M, Peterson C, Andrews P (2009) Stem cell states, fates, and the rules of attraction. *Cell Stem Cell* 4: 387–397.
58. MacArthur B, Ma’ayan A, Lemischka I (2009) Systems biology of stem cell fate and cellular reprogramming. *Nat Rev Mol Cell Biol* 10: 672–681.
59. Müller F, Laurent L, Kostka D, Ulitsky I, Williams R, et al. (2008) Regulatory networks define phenotypic classes of human stem cell lines. *Nature* 455: 401–405.
60. Graf T, Stadtfeld M (2008) Heterogeneity of embryonic and adult stem cells. *Cell Stem Cell* 3: 480–483.
61. Huang S, Guo YP, May G, Enver T (2007) Bifurcation dynamics in lineage-commitment in bipotent progenitor cells. *Dev Biol* 305: 695–713.
62. Chickarmane V, Enver T, Peterson C (2009) Computational modeling of the hematopoietic erythroid-myeloid switch reveals insights into cooperativity, priming, and irreversibility. *PLoS Comput Biol* 5: e1000268.